SAMPLED-DATA MODELING OF SWITCHING REGULATORS

ARTHUR R. BROWN AND R. D. MIDDLEBROOK

California Institute of Technology
Pasadena, California

ABSTRACT

The high-frequency capabilities of two switching regulator modeling techniques, state-space averaging and discrete modeling, are compared. A new linear, small-signal modeling technique, which combines the continuous form of state-space averaging with the accuracy of discrete modeling, is then developed. This new method, called sampled-data modeling, succeeds, where state-space averaging fails, in predicting the subharmonic instability in current-programmed regulators, and is shown to be of significant usefulness in the design of high-performance switching regulators.

1. INTRODUCTION

Switching converters and regulators do not fall into the class of linear, time-invariant circuits to which accurate and straightforward analysis tools, such as the Laplace transform and the Nyquist plot, can be applied. A major goal in the study of these systems, therefore, has been the development of modeling techniques for these circuits. The efforts invested in this area have generally been fruitful, and several new analytical tools are now in use. Two of these methods are the state-space averaging technique of Ćuk [1] and the discrete modeling technique of Packard [2]. Both result in small-signal, linear models, and both make it possible to analyze and design switching converters and regulators. However, each of these methods has a drawback. State-space averaging, while possessing a very convenient continuous, time-invariant form, and having been successful in many applications, is inaccurate when the frequencies of interest approach one-half the fundamental switching frequency of the converter. On the other hand, the discrete modeling technique, while very accurate, requires the abandonment of the usual continuous time model in favor of difference equations, which are unfamiliar to the circuit designer and do not reflect the continuous nature of the converter waveforms.

The purpose of this paper is to compare these existing models, and to introduce a new small-signal, linear modeling technique which incorporates both the continuous form of the state-space averaged model and the high-frequency accuracy of the discrete model. Called the sampled-data modeling technique, this new method also serves as a bridge between the two previously developed methods, allowing the differences between them to be uncovered and appraised. In this capacity, the sampled-data model can serve to indicate when the accuracy of state-space averaging is sufficient for the purposes of a design task, and when its own greater power at high frequencies is required. A block diagram of this new model is shown in Fig. 1.
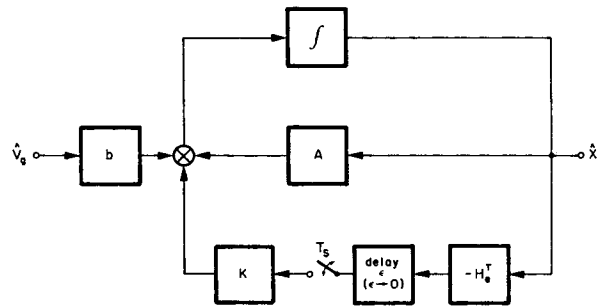

Figure 1. *Block diagram of the sampled-data model.*

The development of this new method begins with a careful second look at the developments of state-space averaging and the discrete modeling technique. In Section 2, a common foundation for these models is developed via a series of manipulations of the state equations of a switching converter. The result is a linear equation describing converter operation. Significantly, the only requirement for the validity of this equation is that any converter perturbations be small. While too complicated to be directly useful, this result can be used as a common starting point for the derivations of state-space averaging and discrete modeling.

Building on this base, Section 3 proceeds to develop the state-space averaging method, noting with care all assumptions used. Both converter and regulator analysis are treated. It is found that two modifications

must be made in order to achieve the state-space averaged form. The first, an averaging of time-varying coefficients, is shown to be related to the well-known *straight-line approximation*, which is valid when the converter's natural frequencies are much lower than its switching frequency, and which is therefore well satisfied for switching converters. The second change requires that the duty ratio modulation function, originally a string of pulses, be smoothed into a continuous function, and is less easily justified. Specifically, this step effectively eliminates a sampler, and hence may be expected to affect the accuracy of state-space averaging at frequencies approaching one-half the switching frequency, a region hereafter known as the "high-frequency" regime. In spite of this defect, however, the literature shows that state-space averaging has a long and successful record in the modeling and design of switching regulator systems.

In comparison, Section 4 treats the development of the discrete modeling technique. It is found that this method can be derived from the result of Section 2 with no further approximations. Thus, it is expected that this model may be more accurate than state-space averaging in the high-frequency region.

These expectations are fulfilled in Section 5, in which a form of converter regulation known as *current-programming* is introduced as a test of modeling methods. This feedback scheme, which has recently become very popular, possesses a potential instability, consisting of a limit cycle at one-half the switching frequency, which occurs when the duty ratio of the controlled converter attempts to exceed one-half. This well-defined instability makes current-programming a natural choice for a comparison of the high-frequency capabilities of the modeling techniques discussed in previous sections. It is found that state-space averaging fails to predict this instability while discrete modeling accurately records it, thus confirming the expectations of the two methods' relative capabilities in the high-frequency region. A more general discussion shows that this kind of difference in prediction exists for a broad class of regulator systems.

The stage is now set for the development of a new modeling technique. In Section 6, *sampled-data modeling*, so named because its form is that of a sampled-data system, is introduced. While the development here is similar to that of state-space averaging, it avoids the unjustified approximation used in the derivation of that model, and so results in a more accurate, yet still continuous and linear, model. The increased accuracy is seen in the ability of the sampled-data technique to predict correctly the occurrence of instability in current-programmed regulators.

In Section 7, a detailed discussion of the sampled-data method is presented, emphasizing its similarities and differences with both state-space averaging and the discrete modeling technique, and displaying some general properties of its loop gain. Sampled-data modeling and discrete modeling are seen to be essentially equivalent representations of the same process, although in any given case one representation may be more convenient to use than the other. On the other hand, the sampled-data and state-space averaged models are seen to differ solely in the presence of a sampler in the new model. Physical and mathematical relationships

are developed which show that the two methods agree at low frequencies, state-space averaging being a limiting case of the more powerful sampled-data technique. Consideration of the sampled-data loop gain reveals several properties of this function, characteristics which make its plotted form quite striking and which provide insight into the design process. Finally, conclusions are presented in Section 8.

2. FUNDAMENTALS OF SWITCHING CONVERTER ANALYSIS

In this section, a linear equation describing the small-signal behavior of switching converters is developed. Adapted from Packard [2], this development invokes only a small-signal assumption, and hence should be accurate in all frequency ranges.

The analysis in this paper, while easily extended to other configurations, will be carried out for constant frequency switching regulators operating in the "continuous conduction" mode, in which no constraints on state variables are effective. Generally, in this operating mode, two different circuit topologies appear in the course of a complete switching cycle. Let $x(t)$ be the state vector, $v_g(t)$ the (nominally dc) source voltage, and T_s the switching period. Then such a converter is characterized by two state equations during a switching cycle.

$$\dot{x} = A_1 x + b_1 v_g \quad , \quad nT_s < t < (n+d_n)T_s \qquad (1a)$$

$$\dot{x} = A_2 x + b_2 v_g \quad , \quad (n+d_n)T_s < t < (n+1)T_s \qquad (1b)$$

$$n = ..., -1, 0, +1, ...$$

Here A_1 and A_2 are square matrices which describe the two circuit topologies, and b_1 and b_2 are vectors that determine the effects of the source v_g. The duty ratio is represented by the fractional quantity d_n, $0 < d_n < 1$.

These two matrix equations can be combined into one by the definition of two switching functions, shown in Fig. 2.
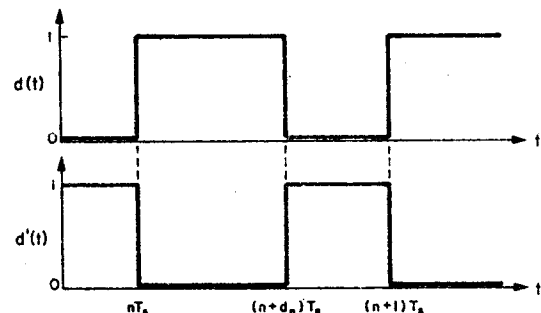

Figure 2. *Definitions of switching functions d(t) and d'(t).*

$$d(t) = \begin{cases} 1 & \text{if } nT_s < t < (n+d_n)T_s \\ 0 & \text{if } (n+d_n)T_s < t < (n+1)T_s \end{cases} \qquad (2a)$$

$$d'(t) = 1 - d(t) \qquad (2b)$$

With use of these functions, a single state equation suffices to describe the converter.

350

$$\dot{x} = [d(t)A_1 + d'(t)A_2]x + [d(t)b_1 + d'(t)b_2]v_g \quad (3)$$

As a brief aside, consider the character of this equation. If d_n is a constant for all n, that is, if the converter is operated at constant duty ratio, without control, then Eq. (3) is a linear equation with periodic coefficients. If, on the other hand, control is exercised, that is, d_n is a function of the state vector x, and possibly v_g as well, then the equation becomes nonlinear.

Since control must be utilized in the design of a regulator, small-signal analysis must be used to obtain a linear equation. For this purpose, assume that the source consists of a dc quantity and a perturbation.

$$v_g(t) = V_g + \hat{v}_g(t) \quad (4)$$

The notation used throughout this paper is that dc or average values are represented by capital letters, and that perturbations are indicated by carets. Similarly, suppose that the duty ratio consists of a constant plus a perturbation.

$$d_n = D + \hat{d}_n \quad (5)$$

Then the switching functions consist of a steady-state, time-varying part and a perturbation. In the notation used here, functions' steady-state forms, which may be time-varying, are denoted by bars.

$$d(t) = \bar{d}(t) + \hat{d}(t) \quad (6a)$$

$$d'(t) = 1 - d(t) \quad (6b)$$

$$\bar{d}(t) = \begin{cases} 1 & \text{if } nT_s < t < (n+D)T_s \\ 0 & \text{if } (n+D)T_s < t < (n+1)T_s \end{cases} \quad (6c)$$

$$\hat{d}(t) = \begin{cases} \text{sgn}(d_n - D) & \text{if } t\,\epsilon[(n+D)T_s, (n+d_n)T_s] \\ 0 & \text{otherwise} \end{cases} \quad (6d)$$

$$\text{sgn}(y) = \begin{cases} +1 & \text{if } y > 0 \\ 0 & \text{if } y = 0 \\ -1 & \text{if } y < 0 \end{cases} \quad (6e)$$

These functions are illustrated in Fig. 3.

As a result of these perturbations, the state vector $x(t)$ will also consist of a steady-state, time-varying part (the state vector in the absence of perturbations) and a perturbation.

$$x(t) = \bar{x}(t) + \hat{x}(t) \quad (7)$$

These expansions are then substituted into the state equation, Eq. (3).

$$\dot{\bar{x}} + \dot{\hat{x}} = [(\bar{d} + \hat{d})A_1 + (\bar{d}' - \hat{d})A_2][\bar{x} + \hat{x}] + [(\bar{d} + \hat{d})b_1 + (\bar{d}' - \hat{d})b_2][V_g + \hat{v}_g] \quad (8)$$

After collection of terms, the steady-state portion can be separated from the perturbation's influence.

$$\dot{\bar{x}} + \dot{\hat{x}} = [\bar{d}A_1 + \bar{d}'A_2]\bar{x} + [\bar{d}b_1 + \bar{d}'b_2]V_g$$
$$+ [\bar{d}A_1 + \bar{d}'A_2]\hat{x} + [\bar{d}b_1 + \bar{d}'b_2]\hat{v}_g \quad (9)$$
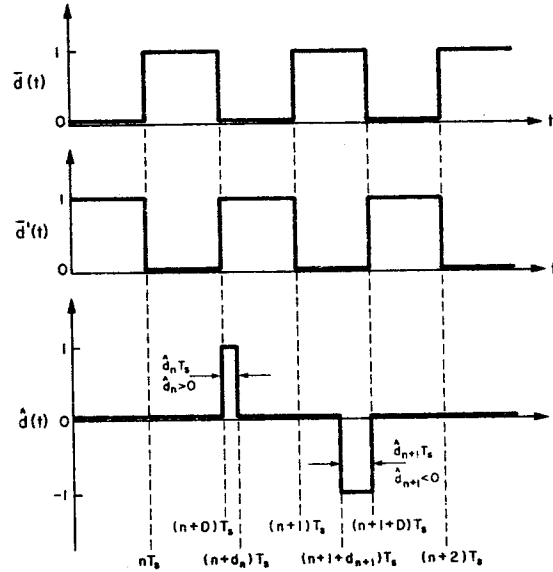$$+ [(A_1-A_2)(\bar{x}+\hat{x})+(b_1-b_2)(V_g+\hat{v}_g)]\hat{d}$$

Figure 3. *Definitions of steady-state switching functions $\bar{d}(t)$ and $\bar{d}'(t)$, and of the perturbation $\hat{d}(t)$.*

If there are no perturbations $(\hat{d}(t) = 0, \hat{v}_g(t) = 0)$, the steady-state equation is obtained.

$$\dot{\bar{x}}(t) = [\bar{d}(t)A_1 + \bar{d}'(t)A_2]\bar{x}(t) + [\bar{d}(t)b_1 + \bar{d}'(t)b_2]V_g \quad (10)$$

The subtraction of Eq. (10) from Eq. (9) results in an equation for the perturbation.

$$\dot{\hat{x}}(t) = [\bar{d}(t)A_1 + \bar{d}'(t)A_2]\hat{x}(t)$$
$$+ [\bar{d}(t)b_1 + \bar{d}'(t)b_2]\hat{v}_g(t)$$
$$+ [(A_1-A_2)\bar{x}(t) + (b_1-b_2)V_g]\hat{d}(t) \quad (11)$$
$$+ [(A_1-A_2)\hat{x}(t) + (b_1-b_2)\hat{v}_g(t)]\hat{d}(t)$$

This equation is then linearized by the assumption that the perturbations are sufficiently small that the products of perturbations in the final term make this quantity's effects negligible compared to the effects of the other terms.

$$\dot{\hat{x}}(t) = [\bar{d}(t)A_1 + \bar{d}'(t)A_2]\hat{x}(t)$$
$$+ [\bar{d}(t)b_1 + \bar{d}'(t)b_2]\hat{v}_g(t)$$
$$+ [(A_1 - A_2)\bar{x}(t) + (b_1 - b_2)V_g]\hat{d}(t) \quad (12)$$

Because of the small-signal restriction, the function $\hat{d}(t)$ now consists of a series of narrow pulses at the times $(n+D)T_s$, of height +1 if $\hat{d}_n > 0$ and -1 if $\hat{d}_n < 0$. This function is approximated very well by a string of delta functions of appropriate areas, as shown in Fig. 4.

$$\hat{d}(t) \approx \hat{p}(t) = \sum_{n=-\infty}^{\infty} \hat{d}_n T_s \, \delta[t - (n+D)T_s] \quad (13a)$$

$$= \hat{u}(t)T_s \sum_{n=-\infty}^{\infty} \delta[t - (n+D)T_s] \quad (13b)$$

Here $\hat{u}(t)$ is any continuous time function which matches $\hat{d}_n$ at the appropriate instants.
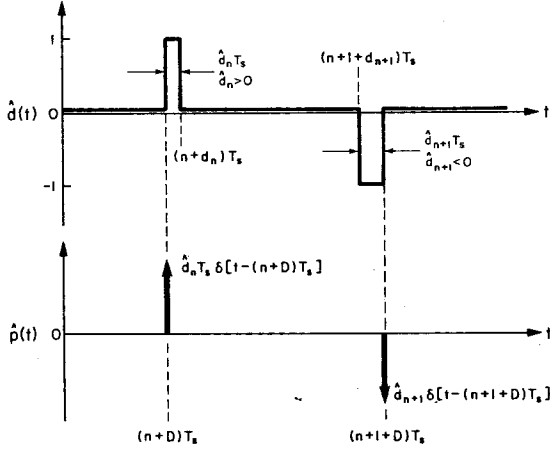
351

Figure 4. *Replacement of $\hat{d}(t)$ by the string of delta functions $\hat{p}(t)$.*

$$\hat{u}[(n+D)T_s] = \hat{d}_n \qquad (14)$$

While this function $\hat{u}(t)$ is not uniquely defined, its existence proves to be useful in the modeling of controllers, where continuous converter waveforms are used to generate the duty ratio modulation. Note the resemblance of Eq. (13) to a sampling operation. This resemblance is exploited heavily in Section 5, in which a new modeling technique is developed.

The string of delta functions $\hat{p}(t)$ can now be substituted for $\hat{d}(t)$ in the small-signal Eq. (12).

$$\hat{x}(t) = [\overline{d}(t)A_1 + \overline{d}'(t)A_2]\hat{x}(t)$$
$$+ [\overline{d}(t)b_1 + \overline{d}'(t)b_2]\hat{v}_g(t) \qquad (15)$$
$$+ [(A_1-A_2)\overline{x}[(n+D)T_s]+(b_1-b_2)V_g]\hat{p}(t)$$

The delta functions pick out only the value of $\overline{x}[(n+D)T_s]$ from $\overline{x}(t)$ in the final term. Because of the small-signal approximation, this equation is linear. However, it is definitely not time-invariant. Furthermore, it is driven by a string of delta functions. To obtain a useful result, further modifications are necessary. In the following sections, various means of simplification will result in the state-space averaging and discrete analysis techniques, as well as the new sampled-data modeling method.

3. REVIEW OF STATE-SPACE AVERAGING

In this section, the state-space averaging modeling technique, originated by Ćuk, is examined, with an emphasis on the method's accuracy at high frequencies. The method of development is not the same as that originally employed [1]; the intent here is to use a common method for several different modeling techniques, in order to better understand their similarities and differences. The section is divided into two subsections, which treat state-space averaging converter modeling and regulator modeling, respectively.

3.1 Converter modeling

The starting point in this development of state-space averaging is the set of results from the previous section, Eqs. (13-15). The only approximation used in the derivation of these results was to assume that the perturbations in the switching function $d(t)$ and input $v_g(t)$ were small, so that nonlinear terms could be neglected and the finite-width pulses of $\hat{d}(t)$ could be replaced by the string of delta functions $\hat{p}(t)$.

Clearly, an existing modeling technique cannot be reproduced without prior knowledge of its form. State-space averaging represents the small-signal behavior of switching converters in terms of a linear time-invariant state equation, driven by a continuous duty ratio modulation function. Now Eq. (15) is linear, but it is definitely not time-invariant, and the driving term consists of a string of delta functions. To arrive at a state-space averaging type of result, some further manipulation is necessary.

Each of the terms of the differential equation in Eq. (15) must be modified in order to obtain a time-invariant result. The first two terms have time-varying coefficients, while the third, driving, term actually samples the continuous signal $\hat{u}(t)$. The simplest way to remedy the situation is to replace the offensive time-varying quantities by their average values. However, this change will certainly result in a loss of accuracy. The following analysis attempts to determine the degree of error introduced.

Suppose first that no duty ratio modulation is present, that is, $\hat{p}(t)=0$. Suppose further that $\hat{v}_g(t)$ consists solely of components which vary slowly with respect to the switching frequency, so that it may be considered constant over a switching period. Then Eq. (15) can easily be solved for the state at time $(n+1)T_s$ in terms of the state at time nT_s, via a two-step integration over the intervals $[nT_s, (n+D)T_s]$ and $[(n+D)T_s, (n+1)T_s]$.

$$\hat{x}[(n+D)T_s] = e^{A_1 D T_s}\hat{x}[nT_s]$$
$$+ \int_{nT_s}^{(n+D)T_s} e^{A_1[(n+D)T_s-\tau]}b_1\hat{v}_g\,d\tau \qquad (16a)$$

$$= e^{A_1 D T_s}\hat{x}[nT_s]$$
$$+ A_1^{-1}(e^{A_1 D T_s} - I)b_1\hat{v}_g \qquad (16b)$$

$$\hat{x}[(n+1)T_s] = e^{A_2 D'T_s}e^{A_1 D T_s}\hat{x}[nT_s]$$
$$+ e^{A_2 D'T_s}A_1^{-1}(e^{A_1 D T_s} - I)b_1\hat{v}_g$$
$$+ \int_{(n+D)T_s}^{(n+1)T_s} e^{A_2[(n+1)T_s-\tau]}b_2\hat{v}_g\,d\tau \qquad (17a)$$

$$= e^{A_2 D'T_s}e^{A_1 D T_s}\hat{x}[nT_s]$$
$$+ e^{A_2 D'T_s}A_1^{-1}(e^{A_1 D T_s} - I)b_1\hat{v}_g \qquad (17b)$$
$$+ A_2^{-1}(e^{A_2 D'T_s} - I)b_2\hat{v}_g$$

Although this result appears complex, it can be reduced to a simple form by an invocation of the extremely useful *straight-line approximation*. This approximation states that, as a result of the requirement that the

switching ripple on the states of a converter be small, the exponential matrices describing the evolution of these states can be accurately represented, in their intervals of validity, by the first two terms of their Taylor series expansions, with all higher order terms neglected. The use of this approximation, together with the neglect of all terms of order greater than T_s, gives a simple yet accurate approximation of Eq. (17).

$$\hat{x}[(n+1)T_s] = [I + (DA_1 + D'A_2)T_s]\hat{x}[nT_s] \\ + (Db_1 + D'b_2)T_s\hat{v}_g \qquad (18)$$

However, this result is precisely the straight-line approximation to the solution of another, more elementary, differential equation.

$$\dot{\hat{x}}(t) = A\hat{x}(t) + b\hat{v}_g(t) \qquad (19a)$$

$$A = DA_1 + D'A_2 \quad , \quad b = Db_1 + D'b_2 \qquad (19b)$$

This equation is both linear and time-invariant, as desired for state-space averaging. In fact, it is the result of the averaging of the time-varying coefficients in the original equation, as suggested earlier. Hence, with little loss in accuracy, Eq. (19) can replace Eq. (15) for the case $\hat{p}(t)=0$, and the original equation has been partly reduced to the state-space averaging form.

The third term of Eq. (15), given explicitly in Eq. (13), remains to be examined. This driving term, which inserts the effects of duty ratio modulation, consists of a string of delta functions, effectively sampling the continuous function $\hat{u}(t)$.

$$K\hat{p}(t) = K \left\{ T_s \sum_{n=-\infty}^{\infty} \delta[t - (n+D)T_s] \right\} \hat{u}(t) \qquad (20)$$

As stated earlier, the state-space averaged model employs a continuous duty ratio modulation function. Hence, it is natural to interpret the function $\hat{u}(t)$ as this input, and to treat the bracketed factor in Eq. (20) as an unwanted (for state-space averaging) time-dependent coefficient. As before, a simple way to remove this offending quantity is to take its time average.

$$\frac{1}{T_s}\int_{kT_s}^{(k+1)T_s} T_s \sum_{n=-\infty}^{\infty} \delta[t - (n+D)T_s]dt = 1 \qquad (21)$$

This step effectively replaces the pulsed duty ratio modulation function $\hat{p}(t)$ in the differential equation by the continuous function $\hat{u}(t)$. Of course, as with the previous modifications of Eq. (15), this change introduces errors into the model, principally in allowing $\hat{u}(t)$ to affect the model at all times, rather than only at a single instant in each switching cycle, as in the original equation. Because of this qualitative change in the nature of the driving term, this modification, in contrast to the previous manipulations, is not easily justified. It may be expected that the effects of this change will become most noticeable for perturbation frequencies approaching one-half the switching frequency of the converter, since this region is where the difference between the pulsed and smoothed duty ratio modulation functions will appear most pronounced.

With these changes, Eq. (15) appears in quite different form.

$$\dot{\hat{x}}(t) = A\hat{x}(t) + b\hat{v}_g(t) + K\hat{u}(t) \qquad (22a)$$

$$A = DA_1 + D'A_2 \ , \ b = Db_1 + D'b_2 \qquad (22b)$$

$$K = (A_1 - A_2)\overline{x}[(n+D)T_s] + (b_1 - b_2)V_g \qquad (22c)$$

$$\hat{d}_n = \hat{u}[(n+D)T_s] \qquad (22d)$$

Except for the appearance of $\overline{x}[(n+D)T_s]$ instead of the average steady-state vector X, this equation is just the state-space averaging model. Indeed, since the ripple on a state waveform is usually much less than the average value of that waveform, the average state X can usually be substituted in Eq. (22) for $x[(n+D)T_s]$. A block diagram of the state-space averaged model is shown in Fig. 5.

Figure 5. *Block diagram of state-space averaged converter model.*

3.2 Controller and regulator modeling

The fact that the converter model is only valid for small perturbations means that the controller equation need only be a small-signal model. Hence, nonlinearities can be neglected in the usual fashion, and duty ratio modulation can be described, in the Laplace transform domain, as a linear combination of possibly processed state waveforms.

$$\hat{U}(s) = -H_e^T \hat{X}(s) \qquad (23)$$

The effective gain vector H_e (the superscript "T" means transposed) may vary with operating point but is fixed once an operating point is chosen. It may contain frequency dependent terms representing, for example, filtering or time delays.

The combination of Eq. (23) with the Laplace transform of the state-space averaging Eq. (22) gives an equation for the duty ratio modulation.

$$\hat{U}(s) = \frac{-H_e^T(sI - A)^{-1}b}{1 + H_e^T(sI - A)^{-1}K}\hat{V}_g(s) \qquad (24)$$

From Eq. (24), a loop gain $T(s)$ can be defined, since by definition the closed-loop poles s_p of a system with loop gain $T(s)$ satisfy $T(s_p)=-1$.

$$T(s) = H_e^T(sI - A)^{-1}K \qquad (25)$$

The stability criterion is that the system is unstable if any of the closed-loop poles s_p lie in the right-half s-plane.

353

The state-space averaging approach has been a very fruitful one [1,3,4,5,6]. The model it presents provides a simple yet accurate picture of converter operation, allowing the confident design of regulator systems. In addition, the linear, time-invariant form of its state equation allows an equivalent linear time-invariant circuit model to be developed, which can then be embedded as an element in a surrounding circuit system.

However, one step in the development of state-space averaging does not seem to be entirely justified. Specifically, the replacement of the pulsed duty ratio modulation function $p(t)$ by the continuous function $u(t)$ seems somewhat questionable. In effect, this replacement of pulses by a smooth function amounts to the elimination of a sampler. For low modulation frequencies compared to the sampling frequency (equal to the switching frequency), the presence or absence of a sampler will have little effect, but for systems whose bandwidths approach half the switching frequency it seems probable that the effects of sampling cannot be safely neglected. Later sections will confirm this expectation.

4. REVIEW OF DISCRETE MODELING

State-space averaging has as its goal the creation of the simplest possible continuous model for the small-signal behavior of switching converters, a linear, time-invariant state equation. In this present chapter a different analysis technique is reviewed. This alternative method, the discrete modeling technique of Packard [2], seeks to describe the small-signal behavior of the converter at only one instant of time during each switching cycle, saying nothing about the waveforms between these points.

The treatment in this chapter parallels that of state-space averaging in Section 3, although the results are of course different. Again two subsections are used to discuss converter and regulator modeling, respectively.

4.1 Converter modeling

The development of the discrete modeling technique begins, as in the case of state-space averaging, with the fundamental Eqs. (13) and (15), rewritten here as Eq. (26).

$$\hat{x}(t) = [\bar{d}(t)A_1 + \bar{d}'(t)A_2]\hat{x}(t)$$
$$+ [\bar{d}(t)b_1 + \bar{d}'(t)b_2]\hat{v}_g(t) \qquad (26a)$$
$$+ [(A_1 - A_2)\bar{x}[(n+D)T_s] + (b_1 - b_2)V_g]\hat{p}(t)$$

$$\hat{p}(t) = \hat{d}_n T_s \sum_{n=-\infty}^{\infty} \delta[t - (n+D)T_s] \qquad (26b)$$

It is important to remember that the only approximation used in the derivation of this equation was the assumption that the perturbations in $d(t)$ and $v_g(t)$ were small, which made the nonlinear terms small enough to be neglected, and which also allowed the replacement of the pulses of $\bar{d}(t)$ by the delta functions of $\hat{p}(t)$. Note also that the continuous, non-unique function $u(t)$ is not introduced in this development.

The derivation begins with the integration of Eq. (26) over a switching period. The starting point of the

integration is arbitrary, but if it is chosen based on the type of controller to be used, the control equation can be simplified. One controller which has been successfully employed [7] uses sample-and-hold techniques: the fed-back signal is sampled at the instants nT_s, and this value, by comparison with a ramp, is used to determine the duty ratio d_n for the n-th cycle. A second method, in widespread use, involves natural sampling, in which the fed-back waveform is compared directly against a ramp to determine the duty ratio. In this case, it is the values of the fed-back state at the instants of switching, $(n+D)T_s$, which determine the duty ratio.

Since, as has been mentioned, discrete modeling gives predictions only for certain instants of time, it is convenient to choose those instants to correspond to those moments at which the fed-back state determines the duty ratio. This choice makes the problem of regulator design simpler. The special instants correspond to the choice of the initial point for the integration of Eq. (26). In this paper, it will be assumed that natural sampling is to be employed, so the integration will begin at the moment $(n+D)T_s$.

The first portion of the integration covers the interval $[(n+D)T_s, (n+1)T_s]$. The state equation in this interval reduces to a simpler form because $\bar{d}(t)=0$ and $\bar{d}'(t)=1$.

$$\hat{x} = A_2\hat{x} + b_2\hat{v}_g + KT_s\hat{d}_n\delta[t-(n+D)T_s] \qquad (27a)$$
$$(n+D)T_s < t < (n+1)T_s$$

$$K = (A_1 - A_2)\bar{x}[(n+D)T_s] + (b_1 - b_2)V_g \qquad (27b)$$

Note that the delta function at $(n+D)T_s$ is included in the integrand for this period, rather than at the end of the previous period. The reason for this procedure is somewhat subtle. In regulator analysis, the duty ratio modulation at time $(n+D)T_s$ is determined by $x[(n+D)T_s]$, the state vector at that instant. If this state value were to include the effects of the duty ratio modulation delta function at time $(n+D)T_s$, the controller would know the results of its actions before they happened, a clear contradiction. To maintain causality in the model, the duty ratio modulation at time $(n+D)T_s$ must be assumed to affect the state only at times later than $(n+D)T_s$, not at $(n+D)T_s$ itself. This consideration is automatically taken into account by the integration procedure chosen.

After this digression, the formal integration of Eq. (27) continues.

$$\hat{x}[(n+1)T_s] = e^{A_2D'T_s}\hat{x}[(n+D)T_s] + e^{A_2D'T_s}KT_s\hat{d}_n$$
$$+ \int_{(n+D)T_s}^{(n+1)T_s} e^{A_2[(n+1)T_s - \tau]}b_2\hat{v}_g d\tau \qquad (28)$$

Note that a problem now arises because of the source modulation v_g. It is not possible to evaluate this integral explicitly. However, since the main point of the discrete modeling technique is to predict stability, not the effects of input variation, the difficulty is eliminated by the condition $v_g=0$, as will be assumed from now on for this method.

$$\hat{x}[(n+1)T_s] = e^{A_2D'T_s}\hat{x}[(n+D)T_s] + e^{A_2D'T_s}KT_s\hat{d}_n \qquad (29a)$$
$$\hat{v}_g(t)=0 \qquad (29b)$$

354

To complete the integration over the remainder of the switching period, it is necessary to examine the form of the differential equation in the interval $[(n+1)T_s, (n+1+D)T_s]$.

$$\dot{\hat{x}} = A_1\hat{x} \quad , \quad (n+1)T_s < t < (n+1+D)T_s \qquad (30)$$

This equation is readily solved.

$$\hat{x}[(n+1+D)T_s] = e^{A_1 DT_s}e^{A_2 D'T_s}\hat{x}[(n+D)T_s] \\ + e^{A_1 DT_s}e^{A_2 D'T_s}KT_s\hat{d}_n \qquad (31)$$

This result is one of the principal findings of the discrete modeling method. It is a difference, as opposed to a differential, equation, and is both linear and shift-invariant, the latter property being the discrete equivalent of time-invariance in continuous equations. The shift-invariance of Eq. (31) is a consequence of its constant coefficients. An important point to notice is that no additional assumptions or approximations were used to derive this result from Eq. (26), in contrast to the derivation of state-space averaging. Thus, it seems that, at least in some sense, discrete modeling is a more natural method for the analysis of switching converters than state-space averaging.

In another sense, however, discrete modeling is distinctly unnatural, since it gives up the continuous methods engineers are accustomed to using, and therefore renders the Laplace transform ineffective. Fortunately, another tool is available for these linear, shift-invariant difference equations. This technique is the z-transform [8], which converts sequences of numbers into analytic functions in a z-plane, much as the Laplace transform converts continuous functions into analytic functions in an s-plane. Some properties of the one-sided z-transform used in this thesis are covered in Appendix A. Application of one of these to the transformation of Eq. (31) gives a corresponding equation in the z-plane.

$$\hat{X}(z) = (zI-M)^{-1}MKT_s\hat{D}(z) + (zI-M)^{-1}z\hat{x}(0) \quad (32a)$$

$$M = e^{A_1 DT_s}e^{A_2 D'T_s} \qquad (32b)$$

Transformed quantities are represented by upper-case letters, with the type of the transform, Laplace or z, denoted by the functional dependence, s or z, respectively.

4.2 Controller and regulator modeling

In a formal sense, controller and regulator modeling in the discrete case are very similar to the corresponding analyses for state-space averaging. Since the converter was analyzed in such a fashion that the instants at which the states are available are the same as the instants at which the duty ratio modulation is determined, a simple expression can be used to account for many feedback schemes.

$$\hat{d}_n = -H_e^T\hat{x}_n \qquad (33)$$

Here subscripts, rather than a specific time, are used with the state vector because the exact time instant within a cycle at which the duty ratio modulation is determined depends on the controller in question. H_e is a vector of effective gains, which may vary with operating

point, but are constants once the operating point is fixed.

The combination of the z-transform of the controller equation, Eq. (33), with the converter equation, Eq. (32) (derived for natural sampling, it should be remembered), gives an expression for the behavior of the duty ratio in response to a state disturbance.

$$\hat{D}(z) = \frac{-H_e^T(zI-M)^{-1}z\hat{x}(0)}{1 + H_e^T(zI-M)^{-1}MKT_s} \qquad (34)$$

From this equation a loop gain $T_z(z)$ can be defined according to the definition that the closed-loop poles z_p of a system satisfy $T_z(z_p)=-1$.

$$T_z(z) = H_e^T(zI-M)^{-1}MKT_s \qquad (35)$$

The stability criterion is that the system is unstable if any of the closed-loop poles z_p lie outside the unit circle in the z-plane.

The development in this section leads to the expectation that the discrete model should give very accurate predictions of switching regulator behavior, and the next section will confirm this belief. Problems with the use of discrete modeling remain, however. One is the lack of insight into the method which generally exists in the minds of engineers. A second drawback is that the discrete method does not represent the converter state vector as the continuous quantity it is. In Section 6, a new modeling technique which eliminates these problems will be developed. First, however, in the next section, the high-frequency capabilities of state-space averaging and discrete modeling will be compared by the use of both methods to analyze a particular form of regulator arrangement known as current-programming.

5. COMPARATIVE ANALYSES OF CURRENT-PROGRAMMED REGULATORS

In this section, the state-space averaging and discrete modeling techniques are applied to the analysis of a type of feedback arrangement known as *current-programming*, which makes a nearly ideal test of the high-frequency capabilities of modeling methods. After this specific comparison, a more general inspection of the relative performances of the techniques is made. Four subsections are contained in this section, containing, respectively, a review of current-programming, the state-space averaged analysis of the method, the corresponding discrete analysis, and the more general discussion.

5.1 Review of current-programming

Current-programmed regulators have become quite popular in recent years, and have been the subjects of extensive research [3,9,10]. The technique is illustrated in Fig. 6, with a boost converter as an example, although the method can be applied to any converter. Basically, a current-programmed circuit uses a controller in which an inductor current is fed back, and in which no artificially generated ramp is employed. Thus the only ramp-like slope is that of the switching ripple on the fed-back inductor current. Note that, as shown in Fig. 6,
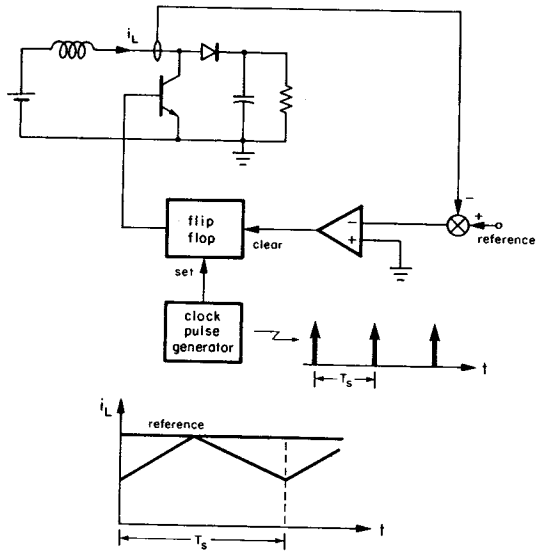
355

Figure 6. *Current-programming applied to a boost converter.*

the current-programmed converter is not, in its elementary form, a voltage regulator; to achieve regulation of the output voltage an additional signal derived from the output is fed back in parallel with the inductor current signal. Equivalently, and as is usually the case in practical systems, the output voltage feedback signal can be added to the reference.

A current-programmed converter has several features which make it quite attractive to designers. First, since the current of the turned-on power transistor is just the fed-back inductor current, a limit on the maximum value of the current reference automatically limits the transistor current, providing built-in protection. Second, several converters can be connected in parallel without any load-sharing problems by the establishment of a single, overall voltage feedback loop, with each component converter receiving the same current reference signal. Third, the low-frequency dynamic characteristic of a current-programmed converter possesses one fewer pole than the same converter without current-programming.

These three features have been studied extensively [3], and will not be discussed here in detail. Instead, another, distinctly disadvantageous, feature of current-programming will be used in this work. This characteristic is the uniform propensity of constant-frequency current-programmed converters to oscillate at one-half the switching frequency when the duty ratio of the power transistor attempts to exceed one-half [3]. Though this phenomenon has been discussed, its nature has seemed somehow different from other converter dynamic behavior, probably because the frequency of oscillation is so high. Usually the analysis of the instability is carried out separately, with different techniques, from low-frequency dynamic analysis [3].

An instability is an instability, however, and whether at low or high frequency, its consequences are usually disastrous. Hence, an accurate modeling technique

should provide predictions of both high-and-low-frequency dynamic behavior, including instabilities. The well-defined nature of the current-programming oscillation (occurring in all the basic converters for duty ratios greater than one-half, at one-half the switching frequency) makes it a natural choice to serve as a test of the high-frequency capabilities of various modeling techniques.

5.2 State-space averaged analysis of current-programming

Consider the current-programming modulator waveforms shown in Fig. 7. From Fig. 7b, the form of the controller equation is easily seen.

(a)

(b) expanded view of (a)

———— steady-state
—·—— perturbed
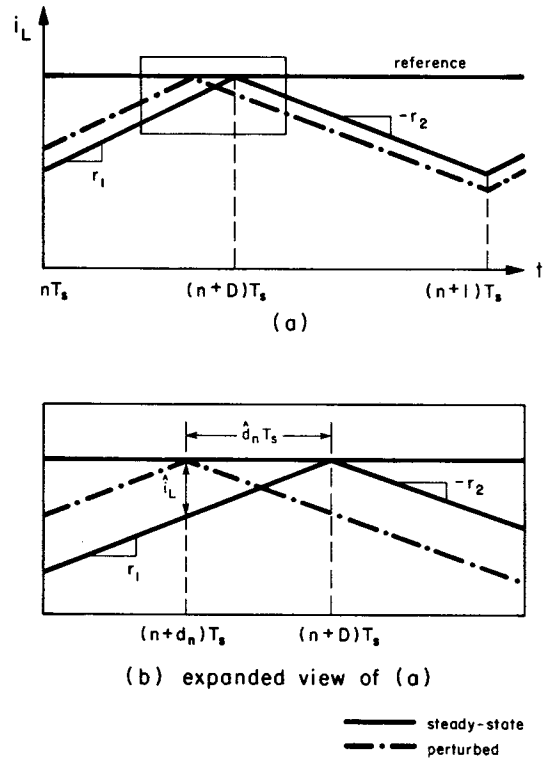
Figure 7. *Current-programming modulator waveforms.*

$$\hat{d}_n T_s = -\frac{\hat{i}_L[(n+D)T_s]}{r_1} \quad , \quad \hat{u} = \frac{\hat{i}_L}{r_1 T_s} \qquad (36)$$

Here r_1 is the slope of the steady-state rising current waveform, and r_2 is the magnitude of the steady-state falling current slope.

The loop gain, as given by Eq. (25) in Section 3, will now be evaluated for a current-programmed regulator. Consider a two-state circuit, the two states being an inductor current i_L and a capacitor voltage v_C.

$$\hat{x} = \begin{bmatrix} \hat{i}_L \\ \hat{v}_C \end{bmatrix} \qquad (37)$$

Now, because the converter is a low-pass system, the dynamics of the state matrix A are low-frequency in nature. In a discussion of a high-frequency phenomenon

such as the subharmonic oscillation of current-programming, these low-frequency effects can be ignored by the substitution $A=0$. This step also generalizes the analysis by making it applicable to any two-state converter, and is in contrast to previous current-programming analysis [3], which concentrated on low-frequency effects and neglected high-frequency terms. From Eq. (23) of Section 3 the effective gain vector H_e can be determined.

$$H_e = \begin{bmatrix} \dfrac{1}{r_1 T_s} \\ 0 \end{bmatrix} \qquad (38)$$

It remains to determine the vector K. Examination of the expression for K in Eq. (22) and the original state equations for the converter, Eq. (1), shows that the components of K are just the differences between the steady-state rates of change of each state variable just before and just after the time $(n+D)T_s$. For the inductor current these slopes are r_1 and $-r_2$, respectively. The other component of K will prove to be irrelevant.

$$K = \begin{bmatrix} r_1 + r_2 \\ - \end{bmatrix} \qquad (39)$$

Substitution of these two equations into the loop gain formula, Eq. (25), with $A=0$, gives an explicit expression for this particular loop gain.

$$T(s) = \frac{r_1 + r_2}{r_1} \frac{1}{sT_s} \qquad (40)$$

Since the closed-loop pole s_p satisfies $T(s_p)=-1$, its location can be easily found.

$$s_p = -\frac{1}{T_s} \frac{r_1 + r_2}{r_1} \qquad (41)$$

This high-frequency pole is the one which appeared to vanish in previous analysis [3], where the order of the system was apparently reduced by one. This disappearance occurred because high-frequency effects were purposely neglected in that study. Conversely, because of the substitution $A=0$, this analysis neglects low-frequency effects, and hence does not uncover the low-frequency pole and zero previously found [3].

The crucial aspect of the pole s_p in Eq. (41) is that it always lies in the left-half s-plane. This position implies a stable system. Hence, state-space averaging has failed to predict the known instability in this feedback technique.

5.3 Discrete analysis of current-programming

The discrete analysis of current-programmed regulators parallels that of state-space averaging exactly, although the results do not. Again, only converters with two state variables are considered, and the state vector is chosen to be the same as before. Examination of the waveforms in Fig. 7 reveals the control law in the discrete modeling format.

$$\hat{d}_n = -\frac{\hat{i}_L[(n+D)T_s]}{r_1 T_s} \qquad (42)$$

Note that the converter model developed in Section 4 gives the states at exactly the instants required by the control law, as desired. The effective feedback gain vector H_e is seen to be identical to the corresponding vector in the state-space averaged analysis.

$$H_e = \begin{bmatrix} \dfrac{1}{r_1 T_s} \\ 0 \end{bmatrix} \qquad (43)$$

Similarly, the vector K is the same as in the state-space averaged case.

$$K = \begin{bmatrix} r_1 + r_2 \\ - \end{bmatrix} \qquad (44)$$

As before, only one component is significant for this calculation. Finally, because the dynamics represented by the M matrix in Eq. (32) are much slower than the sought-after high-frequency phenomena, this matrix is approximated by the unit matrix.

$$M = e^{A_1 DT_s} e^{A_2 D'T_s} \approx I \qquad (45)$$

This step is equivalent to the substitution $A=0$ in the state-space averaged analysis. The loop gain $T_z(z)$ can now be easily found.

$$T_z(z) = \frac{r_1 + r_2}{r_1} \frac{1}{z-1} \qquad (46)$$

The rates of change r_1 and r_2 may be replaced by the duty ratio by means of a relationship which can be derived from Fig. 7.

$$Dr_1 = D'r_2 \qquad (47a)$$
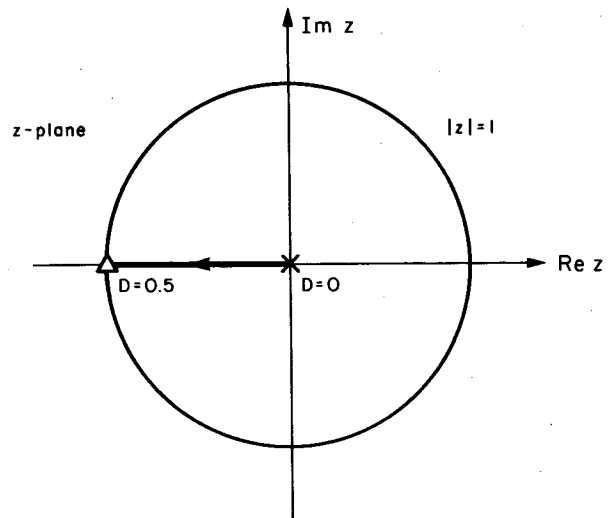
$$\frac{r_2}{r_1} = \frac{D}{D'} \qquad (47b)$$

Figure 8. *Root locus of discrete modeling current-programming pole.*

357

Substitution of this relation into Eq. (48) gives a simple result.

$$T_z(z) = \frac{1}{D'}\frac{1}{z-1} \qquad (48)$$

The closed-loop pole z_p satisfies $T_z(z_p)=-1$, and is easily evaluated.

$$z_p = -\frac{D}{D'} \qquad (49)$$

The locus of this pole as a function of duty ratio is shown in Fig. 8. It is seen that even this approximate discrete modeling analysis reveals a subharmonic instability when the duty ratio reaches 0.5, exactly the behavior seen in actual current-programmed regulators.

The appearance of only one pole, while the original system had two states, is a consequence of the choice $M=I$, just as the substitution $A=0$ in the state-space averaged analysis of current-programming gave only a single pole. In reality there are two poles, but one is close to a zero, near $z=1$, as shown in Fig. 9. The choice $M=I$ makes this pole cancel exactly with the zero, but the cancellation is not perfect for a non-unity M. In addition, a non-unity M may affect the critical duty ratio at which the converter goes unstable.
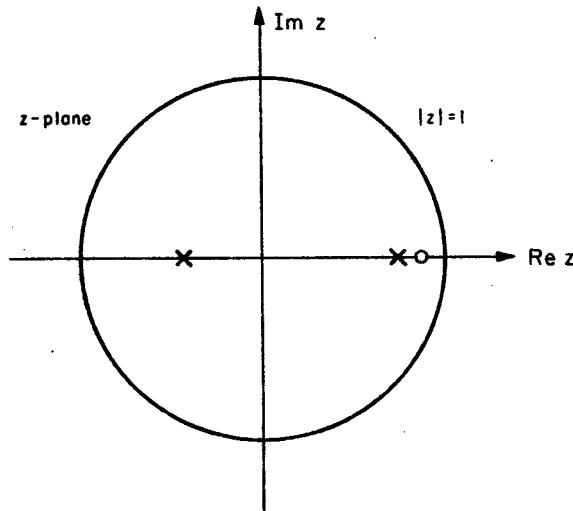
Figure 9. *Actual pole locations for a current-programmed regulator.*

It has been found that if the ramp formed by the inductor current is supplemented by an artificial ramp, the subharmonic instability can be removed [3]. In fact, a particular choice of artificial ramp slope has been shown to eliminate any current error in one switching cycle. This compensation technique can also be analyzed with use of the discrete modeling technique. Consider the current-programmed modulator of Fig. 10, to which an artificial ramp of slope r_R has been added. From this figure, a new control law is easy to determine.

$$\hat{i}_L[(n+D)T_s] = -(r_1+r_R)\hat{d}_n T_s \qquad (50a)$$

$$\hat{d}_n = -\frac{\hat{i}_L[(n+D)T_s]}{(r_1+r_R)T_s} \qquad (50b)$$

(a)
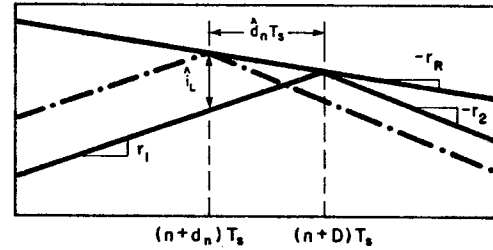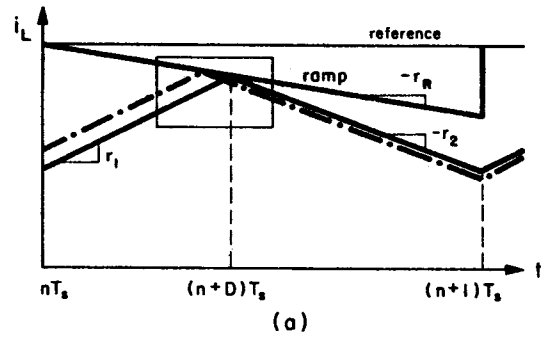
(b) expanded view of (a)

steady-state
perturbed

Figure 10. *Current-programming waveforms in the presence of an artificial ramp.*

The loop gain for this case can be evaluated by use of this new control law in place of the old one.

$$T_z(z;r_R) = \frac{r_1+r_2}{r_1+r_R}\frac{1}{z-1} \qquad (51)$$

The new closed-loop pole location is also easily found.

$$z_p = \frac{r_R-r_2}{r_R+r_1} \qquad (52)$$

Examination of this equation shows that the choice $r_R=r_2$ places the pole exactly at the origin of the z-plane, corresponding to the elimination of current errors in one cycle, as illustrated in Appendix A. This result is exactly that found previously [3].

A few more words on current-programmed systems are appropriate at this point. By itself, a current-programmed circuit does not constitute a voltage regulator; the output voltage must be fed back in addition to the inductor current to achieve output regulation. This system can be analyzed as a multi-loop feedback problem; however, since the current feedback loop is already determined, another approach is to treat the current-programmed circuit as a new plant about which voltage feedback is to be applied, as illustrated in Fig. 11. Here the gain h_1 is already chosen via the current-programming and any artificial ramp used; only h_2 is to be determined. The effects of variations in h_2 on the system dynamics can be explored with the use of a root locus diagram. The "open-loop" poles of this root locus, that is, the poles when h_2 is zero, are just the closed-loop
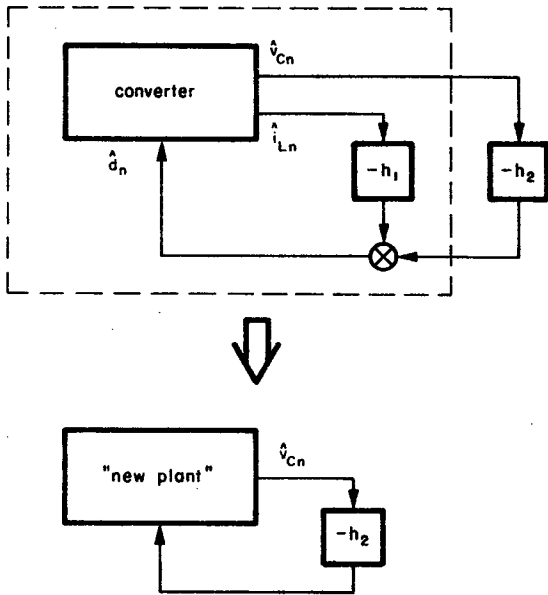
358

Figure 11. *Addition of voltage feedback to a current-programmed regulator.*

poles of the current-programmed circuit, since this closed-loop system is the "plant" for the voltage feedback analysis. The zeros of the voltage feedback loop gain are determined by the details of the converter in question. A possible resulting root locus is shown in Fig. 12. In this example, the high-frequency "open-loop" pole is seen to lie roughly halfway between the z-plane origin and the unstable point $z = -1$, and the loop gain zero is assumed to lie outside the unit circle. As the gain h_2 increases, the system poles migrate according to the usual root locus rules. Note in particular that both poles are headed for the unit circle. The point at which one of them first touches the unit circle marks the onset of instability.
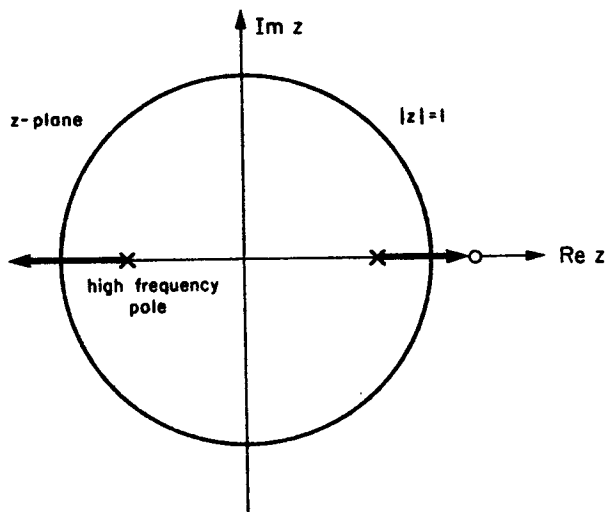
Figure 12. *Possible root locus when voltage feedback is added to a current-programmed regulator.*

An important aspect of this example is that, in the discrete analysis, the high-frequency pole behaves just like any other pole. There is nothing magical about it. In particular, this analysis shows that it is misleading to think that it is possible to position the high-frequency pole via current-programming and then, independently, apply voltage feedback to obtain a regulator; this point of view neglects the effects of the voltage feedback on the high-frequency pole, which migrates like any other pole when feedback is applied. Thus, it is entirely possible that a current-programmed regulator designed to be stable in the absence of voltage feedback will develop a subharmonic instability if excessive voltage feedback is applied.

Thus far, the emphasis in this section has been placed on the differences between state-space averaging and discrete modeling predictions for current-programmed circuits. However, the qualitative differences in results given by the two techniques are not limited solely to this one application. Indeed, it is easy to see that any regulator whose state-space averaged loop gain looks like a single pole at high frequencies will be expected, according to state-space averaging, to have no high-frequency instabilities, but that the corresponding discrete model of the system will predict subharmonic oscillations if the gain of the loop is made too large. This difference is illustrated in Fig. 13.
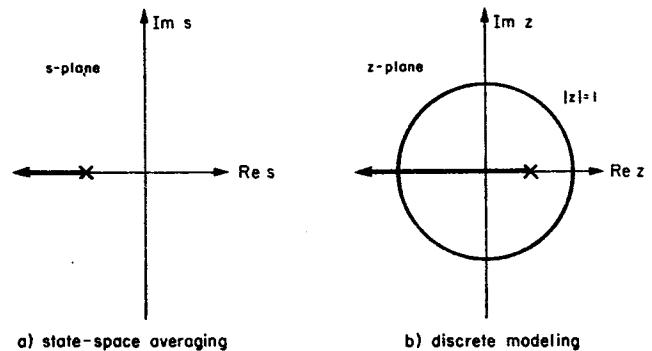

Figure 13. *Comparison of state-space averaged and discrete root loci for a single pole system.*

The comparisons of this section have demonstrated that state-space averaging develops inaccuracies at high frequencies, while discrete modeling remains accurate. However, the problems with the use of the discrete method, which were discussed earlier, remain. What is clearly needed is a modeling technique which possesses the continuous form of state-space averaging, while retaining the accuracy of discrete modeling. In the next section, such a technique is introduced.

6. SAMPLED-DATA MODELING

As stated in the previous section, it is desirable to have a modeling technique which possesses the continuous form of state-space averaging and the accuracy of discrete modeling. This section develops such a model and demonstrates its accuracy by applying it to current-programmed regulators.

6.1 Converter modeling

Both the state-space averaging and the discrete models were developed from the same equations, Eqs. (13) and (15), repeated here as Eq. (53).

$$\dot{\hat{x}}(t) = [\overline{d}(t)A_1 + \overline{d}'(t)A_2]\hat{x}(t)$$
$$+ [\overline{d}(t)b_1 + \overline{d}'(t)b_2]\hat{v}_g(t) \qquad (53a)$$
$$+ [(A_1-A_2)\overline{x}[(n+D)T_s] + (b_1-b_2)V_g]\hat{p}(t)$$

$$\hat{p}(t) = \sum_{n=-\infty}^{\infty} \hat{d}_n T_s \delta[t-(n+D)T_s]$$
$$= \hat{u}(t)T_s \sum_{n=-\infty}^{\infty} \delta[t-(n+D)T_s] \qquad (53b)$$

The only approximation used in the derivation of this equation was to assume that all perturbations about the steady state are small. The discrete modeling technique made no further approximations in arriving at its final form, but state-space averaging, it will be recalled, required some additional modifications. It is not too surprising then, that the predictions of the two models differ.

Two steps were necessary to convert Eq. (53) into the form of state-space averaging. The first was to retain only the average values of $\overline{d}(t)A_1 + \overline{d}'(t)A_2$ and $\overline{d}(t)b_1 + \overline{d}'(t)b_2$, dropping the components at and above the switching frequency. The second step was to smooth out the pulsed nature of the driving term $\hat{p}(t)$, converting it into a continuous function. It is natural to ask whether one of these steps was more responsible than the other for the degradation of the ability of state-space averaging to predict the subharmonic oscillations of current-programmed regulators. This question will be answered in this section by consideration of a model which, in a sense, lies between the state-space averaging and the discrete modeling techniques.

The new model is obtained by use of only one of the two approximations adopted in the development of state-space averaging. Specifically, the time-varying components of $\overline{d}(t)A_1 + \overline{d}'(t)A_2$ and $\overline{d}(t)b_1 + \overline{d}'(t)b_2$ are neglected, but $\hat{p}(t)$ is not modified. Recall that in Section 3, this first step was shown to be related to the straight-line approximation, a good assumption, while the modification of $\hat{p}(t)$ was less well justified. A new state equation is thereby obtained.

$$\dot{\hat{x}}(t) = A\hat{x}(t) + b\hat{v}_g(t) + K\hat{p}(t) \qquad (54a)$$

$$A = DA_1 + D'A_2, \quad b = Db_1 + D'b_2 \qquad (54b)$$

$$K = (A_1-A_2)\overline{x}[(n+D)T_s] + (b_1-b_2)V_g \qquad (54c)$$

$$\hat{p}(t) = \sum_{n=-\infty}^{\infty} \hat{d}_n T_s \delta[t-(n+D)T_s]$$
$$= \hat{u}(t)T_s \sum_{n=-\infty}^{\infty} \delta[t-(n+D)T_s] \qquad (54d)$$

A simple time translation is now performed so that the pulses occur at times nT_s, a standard form.

$$\dot{\hat{x}}(t) = A\hat{x}(t) + b\hat{v}_g(t) + K\hat{p}(t) \qquad (55a)$$

$$\hat{p}(t) = \sum_{n=-\infty}^{\infty} \hat{d}_n T_s \delta[t-nT_s]$$
$$= \hat{u}(t)T_s \sum_{n=-\infty}^{\infty} \delta[t-nT_s] \qquad (55b)$$

The time translation is assumed to be understood; the notation for the functions involved is unchanged, as are the values of A, b, and K.

This model is called the *sampled-data model* because it has exactly the form of a sampled-data system. In such an entity, continuous signals flow through a continuous system, except for one or more points where signals are applied only at equally spaced time intervals, with no information being received between the samples. The equation is linear, but, if $\hat{u}(t)$ is considered to be the input, it is not time-invariant, since a translation in $\hat{u}(t)$ by anything other than a multiple of T_s will not result in simply a corresponding shift in the original output. A block diagram of the system is shown in Fig. 14. Here the definition of sampling a signal $\hat{u}(t)$ to obtain a sampled signal $\hat{u}^*(t)$ is slightly different from the usual practice.
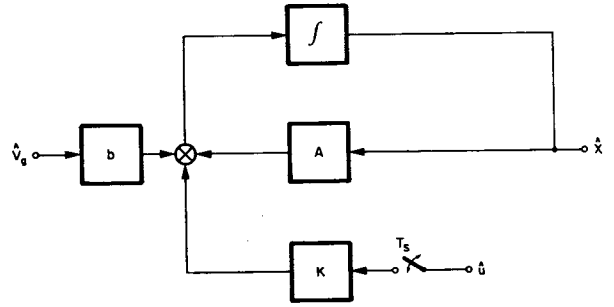

Figure 14. *Block diagram of sampled-data model.*

$$\hat{u}^*(t) = \hat{u}(t)T_s \sum_{n=-\infty}^{\infty} \delta[t-nT_s] \qquad (56)$$

The individual delta functions each has a weight $\hat{u}(nT_s)T_s$, not just $\hat{u}(nT_s)$.

Since the sampled-data model results in a continuous system, the appropriate analysis tool to employ is the Laplace transform, as it was for state-space averaging. In the present case, however, some new transform relations must be developed to deal with the pulse strings which occur in the driving term $\hat{p}(t)$. Appendix B presents some important formulas in this regard. The symbol $V^*(s)$ will denote the Laplace transform of a sampled signal $v^*(t)$, whose original, unsampled waveform was $v(t)$, with Laplace transform $V(s)$.

6.2 Controller and regulator modeling

The block diagram of Fig. 14 suggests that, as for state-space averaging, a good controller model will construct the function $u(t)$ as a linear combination of signals obtained by filtering and other processing of the states. However, in this case, care must be taken

360

because of the presence of the delta functions produced by the sampler. These spikes have an instantaneous effect at the output of the integrator block of Fig. 14, and hence their effects can potentially influence their own creation, much as an incorrect handling of these pulses in Section 4 could have given an incorrect discrete model. In fact, if the problem in the sampled-data model is simply ignored, a non-causal system will result. To eliminate this defect, a small time delay ε is included in the modulator path; this delay, which is eventually allowed to go to zero, prevents the instantaneous transmission of the delta functions' influences and hence restores causality. With this addition, the controller model can be stated.

$$\hat{u}(t) = -H_e^T \hat{x}(t-\varepsilon) \tag{57a}$$

$$\hat{U}(s) = -H_e^T e^{-\varepsilon s}\hat{X}(s) \tag{57b}$$

The Laplace transform of Eq. (55) provides the plant description.

$$\hat{X}(s) = (sI-A)^{-1}b\hat{V}_g(s) + (sI-A)^{-1}K\hat{U}^*(s) \\ + (sI-A)^{-1}\hat{x}(0) \tag{58}$$

When combined, Eqs. (57) and (58) give an expression for the duty ratio modulation as a function of input voltage and initial state perturbation.

$$\hat{U}^*(s) = -H_e^T[e^{-\varepsilon s}\hat{X}(s)]^* \tag{59a}$$

$$= -H_e^T[e^{-\varepsilon s}(sI-A)^{-1}b\hat{V}_g(s)]^* \\ - H_e^T[e^{-\varepsilon s}(sI-A)^{-1}K\hat{U}^*(s)]^* \tag{59b}$$

$$-H_e^T[e^{-\varepsilon s}(sI-A)^{-1}]^*\hat{x}(0)$$

A result stated in Appendix B allows the sampled Laplace transform $\hat{U}^*(s)$ to be removed from any additional sampling, and hence this equation can be solved for $\hat{U}^*(s)$.

$$\hat{U}^*(s) = \frac{-H_e^T[e^{-\varepsilon s}(sI-A)^{-1}b\hat{V}_g(s)]^*}{1 + H_e^T[e^{-\varepsilon s}(sI-A)^{-1}]^*K} \tag{60}$$

Here a zero initial state is assumed. From Eq. (60), a loop gain $T_s^*(s)$ can be defined.

$$T_s^*(s) = H_e^T[e^{-\varepsilon s}(sI-A)^{-1}]^*K \tag{61}$$

The subscript "s" is necessary to distinguish this loop gain from the sampled version of the state-space averaged loop gain $T(s)$. The solutions of the equation $1+T_s^*(s)=0$ are the closed-loop poles s_p of the system. As mentioned previously, when a set of calculations involving these quantities is completed, the artificial delay ε is allowed to go to zero. This limit is understood in Eq. (61) and in all subsequent expressions.

6.3 Sampled-data analysis of current-programming

The steps involved in a sampled-data analysis of a current-programmed switching regulator are, as in the discrete case, completely parallel to those for a state-space averaged analysis. First, low-frequency effects are neglected, a step which also makes the analysis applicable to all converters with two state variables.

$$A = 0 \tag{62}$$

Next, the effective feedback gain vector and the relevant part of the forcing vector are calculated.

$$H_e = \begin{bmatrix} \dfrac{1}{r_1 T_s} \\ 0 \end{bmatrix} \tag{63a}$$

$$K = \begin{bmatrix} r_1 + r_2 \\ - \end{bmatrix} \tag{63b}$$

Finally, the sampled-data loop gain is evaluated from Eq. (61).

$$T_s^*(s) = \frac{1}{T_s}\left(\frac{e^{-\varepsilon s}}{s}\right)^* \frac{r_1 + r_2}{r_1} \tag{64}$$

From Appendix B, the appropriate sampled Laplace transform can be found.

$$\left(\frac{e^{-\varepsilon s}}{s}\right)^* = \frac{T_s}{e^{sT_s} - 1} \tag{65}$$

Thus, an explicit form of the loop gain can be constructed.

$$T_s^*(s) = \frac{r_1 + r_2}{r_1} \frac{1}{e^{sT_s} - 1} \tag{66}$$

The positions of the closed-loop poles s_p can be determined as the roots of $T_s^*(s_p)=-1$.

$$e^{s_p T_s} = -\frac{r_2}{r_1} = -\frac{D}{D'} \tag{67}$$

Here the last equality makes use of Eq. (47). There are infinitely many solutions to this equation.
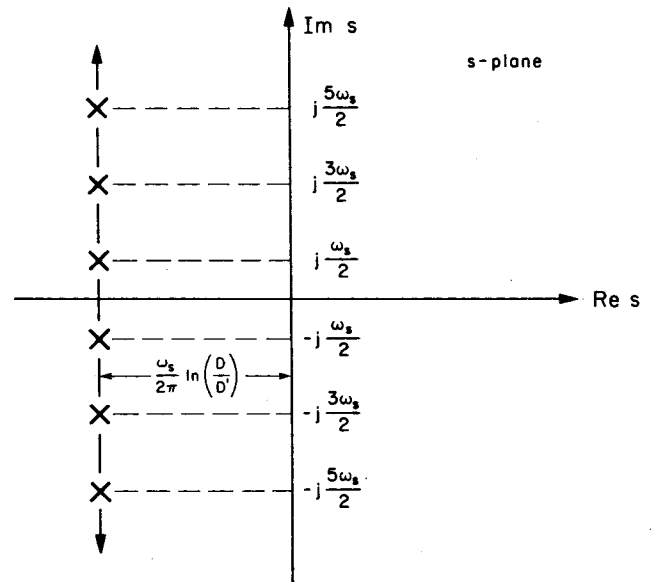

Figure 15. *Current-programming poles from a sampled-data analysis.*

$$s_p = \frac{1}{T_s} \ln\left(-\frac{D}{D'}\right) = \frac{\omega_s}{2\pi} \ln\left(\frac{D}{D'}\right) + j(n+\tfrac{1}{2})\omega_s \quad (68)$$

$$n = 0, \pm 1, \pm 2, \ldots$$

A plot of these poles in the s-plane appears in Fig. 15.

It is easily verified that for $D < D'$, that is, for duty ratios less than 0.5, the real parts of these poles are all negative, indicating a stable system with all poles in the left-half s-plane. Conversely, for duty ratios greater than 0.5, $D > D'$, and the poles lie in the right-half s-plane, implying an unstable system. This prediction matches exactly the observed behavior of current-programmed regulators.

Thus, the goal of a modeling technique with the continuous form of state-space averaging and the accuracy of discrete modeling has been realized in the sampled-data model. In the next section, this new model will be compared extensively to its precursors, with results that allow easy transformation from one to another, and permit greater understanding of all.

7. SAMPLED-DATA MODELING AND ITS RELATIONSHIPS WITH DISCRETE MODELING AND STATE-SPACE AVERAGING

The previous section introduced a new modeling technique, sampled-data modeling, which possesses a continuous form like that of state-space averaging, yet which displays accuracy, at least for current-programmed regulators, comparable to that of discrete modeling. The purpose of the present section is to explore the relationships between this new technique and the two previously known methods, displaying their similarities and differences, and showing how to transform between them. In addition, some general properties of the sampled-data loop gain will be developed. In this section, current-programming is no longer given special treatment; the results achieved here are applicable to many kinds of switching regulator systems.

7.1 Sampled-data modeling versus discrete modeling

The comparison between the sampled-data and discrete methods can be carried out in both the time and transform domains. Consider first the time domain. To compare the sampled-data method with the discrete method, it is necessary to integrate the sampled-data equation over one switching period. The appropriate sampled-data equation, obtained from Eq. (54), is stated here as Eq. (69). The source perturbation v_g is taken to be zero, in accordance with the discrete model's assumptions.

$$\hat{\dot{x}} = A\hat{x} + K\hat{d}_n T_s \delta[t-(n+D)T_s] \quad (69)$$
$$(n+D)T_s < t < (n+1+D)T_s$$

The integration is straightforward.

$$\hat{x}[(n+1+D)T_s] = e^{AT_s}\hat{x}[(n+D)T_s] + e^{AT_s}KT_s\hat{d}_n \quad (70)$$

Compare this result with the corresponding expression for discrete modeling, Eq. (31), repeated here as Eq. (71).

$$\hat{x}[(n+1+D)T_s] = e^{A_1 DT_s}e^{A_2 D'T_s}\hat{x}[(n+D)T_s] \\ + e^{A_1 DT_s}e^{A_2 D'T_s}KT_s\hat{d}_n \quad (71)$$

The sole difference is the replacement of the expression $e^{A_1 DT_s}e^{A_2 D'T_s}$ by the matrix $e^{AT_s} = e^{DA_1 T_s + D'A_2 T_s}$. This replacement is justified by the straight-line approximation, since both expressions have the same first-order expansions.

$$e^{A_1 DT_s}e^{A_2 D'T_s} \approx (I + A_1 DT_s)(I + A_2 D'T_s) \quad (72a)$$
$$\approx I + A_1 DT_s + A_2 D'T_s \quad (72b)$$
$$= I + AT_s \quad (72c)$$
$$\approx e^{AT_s} \quad (72d)$$

Because the straight-line approximation is an excellent assumption for switching converters, the two methods are virtually equivalent in the time domain.

Similarly, in the transform domain, a close relationship exists between the sampled-data loop gain $T_s^*(s)$ and the discrete loop gain $T_x(z)$. As reviewed in Appendix C, if these two loop gains truly represent the same system, the change of variables $z = e^{sT_s}$ should transform one into the other. The sampled-data loop gain $T_s^*(s)$ is given by Eq. (61), repeated here as Eq. (73).

$$T_s^*(s) = H_e^T[e^{-\varepsilon s}(sI-A)^{-1}]^* K \quad (73)$$

Recall that the delay ε is required to preserve causality, and is eventually allowed to go to zero. This equation can be manipulated into a different but equivalent form. If the numbers $v(nT_s)$ are the sampled values of a function $v(t)$, the sampled waveform's Laplace transform can be written as an infinite series involving these values. This expression is stated in Appendix B, and is repeated here as Eq. (74).

$$V^*(s) = T_s \sum_{n=0}^{\infty} v(nT_s)e^{-snT_s} \quad (74)$$

The time function corresponding to the Laplace transform $(sI-A)^{-1}$ in Eq. (73) is easily obtained from consideration of an appropriate matrix differential equation.

$$\dot{m} = Am \quad ; \quad m(0)=I \quad (75a)$$
$$M(s) = (sI-A)^{-1} \quad (75b)$$
$$m(t) = \begin{cases} 0 & \text{if } t < 0 \\ e^{At} & \text{if } t \geq 0 \end{cases} \quad (75c)$$

The values of the matrix function $m(t)$ at times nT_s are not precisely the numbers to be inserted in Eq. (74), however; the delay $e^{-\varepsilon s}$ present in Eq. (73) adds a lag in the time sequence, causing the first term of the series in Eq. (74) to vanish.

$$[e^{-\varepsilon s}(sI-A)^{-1}]^* = T_s \sum_{n=1}^{\infty} e^{A(nT_s-\varepsilon)}e^{-nsT_s} \quad (76a)$$
$$= T_s e^{-\varepsilon A}(I - e^{AT_s}e^{-sT_s})^{-1}e^{AT_s}e^{-sT_s} \quad (76b)$$
$$= T_s(e^{sT_s}I - e^{AT_s})^{-1}e^{AT_s} \quad (76c)$$

In the last step the delay ε was allowed to go to zero, having served its purpose in eliminating the first term of the series. The loop gain $T_s^*(s)$ can now be written in this new form.

$$T_s^*(s) = H_e^T(e^{sT_s}I - e^{AT_s})^{-1}e^{AT_s}KT_s \qquad (77)$$

This expression can be directly compared with that for the discrete loop gain $T_z(z)$, Eq. (35), repeated here as Eq. (78).

$$T_z(z) = H_e^T(zI - M)^{-1}MKT_s \qquad (78a)$$

$$M = e^{A_1 D T_s}e^{A_2 D'T_s} \qquad (78b)$$

It is assumed that the two models are defined such that the effective feedback gain vectors H_e are the same. Then if, as in the time domain discussion, the straight-line approximation is valid, that is, $M \approx e^{AT_s}$, the two loop gains are related by the change of variables $z = e^{sT_s}$, and are two equivalent representations of the same system. Hence, their stability predictions will be nearly identical.

Thus, in both the time and transform domains, the only difference between the sampled-data model and the discrete model was found to be the straight-line approximation. This result should not be surprising: while discrete modeling uses only a small-signal assumption, the sampled-data method invokes the straight-line approximation as well. Hence, results like those found here should be expected.

Another feature is that, in actual calculations with the discrete modeling technique, the straight-line approximation is generally used to compute the matrix M. In such cases, the sampled-data and discrete representations of the loop gain become completely equivalent, and either representation can be used. The close relationship between the sampled-data model and state-space averaging, to be discussed in the next subsection, provides one example where use of the sampled-data model is more convenient.

7.2 Sampled-data modeling versus state-space averaging

The relationships between sampled-data modeling and discrete modeling occur strictly on an abstract, functional level, since the two representations have completely different forms. However, both the sampled-data and the state-space averaged models are continuous in nature, and it may be expected that more physical relationships exist between these two techniques.

Indeed, a comparison of the Laplace-transformed block diagrams of the two in Fig. 16 reveals just such a relationship. These figures are adapted from Figs. 5 and 14, but include the feedback paths not previously shown. The only substantial difference between the two block diagrams is the presence of the sampler in the sampled-data diagram. All of the differences between the two models can therefore be ascribed to this element, and one model can be transformed into the other by the addition or removal of this sampler, together with the addition of the delay ε, if necessary, to maintain causality.
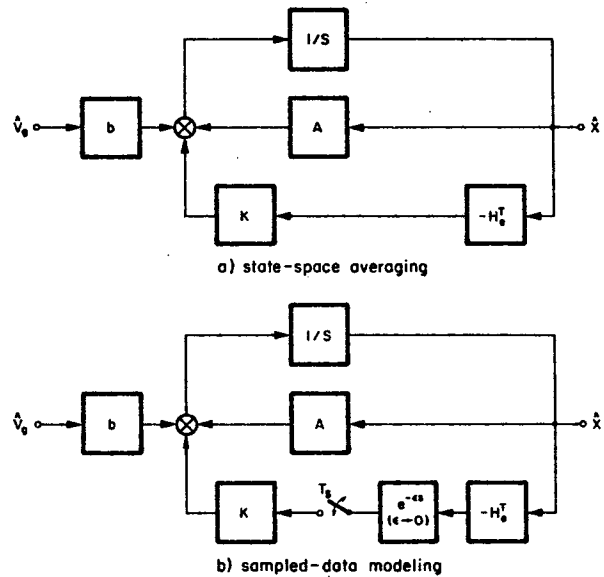
A similar comparison can be made of the time domain

a) state-space averaging

b) sampled-data modeling

Figure 16. *Comparison of block diagrams of state-space averaging and sampled-data modeling.*

equations for the two models, adapted from Eqs. (22) and (55), and rewritten here as Eq. (79).

$$\dot{\hat{x}} = A\hat{x} + b\hat{v}_g + K\hat{u} \quad \text{(state-space averaging)} \qquad (79a)$$

$$\dot{\hat{x}} = A\hat{x} + b\hat{v}_g + K\hat{u}^* \quad \text{(sampled-data modeling)} \qquad (79b)$$

$$\hat{u}^* = \hat{u}(t)T_s \sum_{n=-\infty}^{\infty} \delta[t - nT_s] \qquad (79c)$$

Again the difference between the two models is seen to lie in the sampled-data equation's pulsed driving waveform, which does not appear in the state-space averaged result.

Finally, a comparison of the two methods in the frequency domain can be undertaken. The loop gains for the two techniques are given in Eq. (80), adopted from Eqs. (25) and (61).

$$T_e(s) = H_e^T e^{-\varepsilon s}(sI - A)^{-1}K \quad \text{(state-space)} \qquad (80a)$$

$$T_s^*(s) = H_e^T[e^{-\varepsilon s}(sI - A)^{-1}]^*K \quad \text{(sampled-data)} \qquad (80b)$$

Here a small delay ε has been included in the state-space averaging result to stress its similarity with the sampled-data analysis. This addition does not affect the state-space averaged loop gain as it does the sampled-data one; there are no delta functions driving the state-space averaged equation, so infinitely fast signal propagation through the integrator is not a problem and causality is already firmly established. Thus, when ε is made to go to zero, it will leave no effect on the state-space averaged loop gain.

With this slight modification, the sampled-data loop gain is just the sampled version of the state-space averaged loop gain.

$$T_s^*(s) = [T_e(s)]^* \qquad (81)$$

363

In Appendix B, a relationship, repeated here as Eq. (82), between the Laplace transform of a sampled function and that of its unsampled version is stated.

$$[T(s)]^* = \sum_{n=-\infty}^{\infty} T(s+jn\omega_s) \qquad (82)$$

This relationship is illustrated in Fig. 17 for a low-pass function $T(s)$, like those usually encountered in switching regulator analyses. As can be seen from the figure, at frequencies well below one-half the switching frequency the two functions agree almost exactly. Discrepancies only arise at relatively high frequencies, where overlap between successive "reflections" of the loop gain becomes significant. Thus, state-space averaging can be viewed as a limiting case of the more powerful sampled-data technique; the state-space averaged results are valid in situations where the system bandwidth is well below one-half the switching frequency.
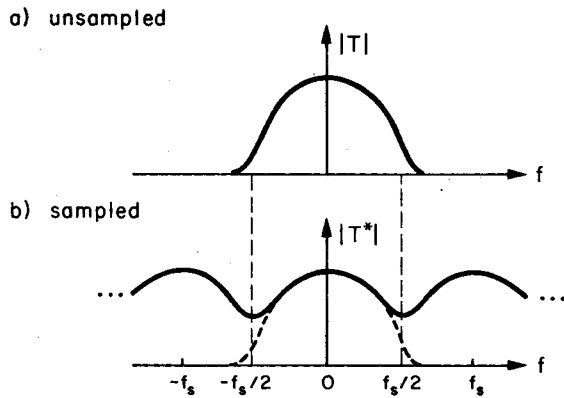
a) unsampled

b) sampled

Figure 17. *Relation between sampled and unsampled Laplace transforms.*

This result demonstrates that it is not always necessary to use the sampled-data model in the design of a regulator system. In many cases, the system bandwidth is limited to a value much less than the switching frequency by characteristics of the converter or controller. One example of such a characteristic is the existence of a right-half-plane zero in the loop gain. The differences between the state-space averaged and sampled-data models are superfluous here: the loop gain must be far below unity gain well before one-half the switching frequency, but, as was just shown, the sampled-data and state-space averaged loop gains diverge only at high frequencies.

The usefulness of the sampled-data analysis occurs when state-space averaging predicts stability even for system bandwidths very close to one-half the switching frequency. A common instance of this situation is that of a state-space averaged loop gain which looks like a single pole at high frequencies, and which therefore predicts stability for any value of gain. Consider such a single-pole loop gain.

$$T(s) = \frac{2\pi f_c}{s} \qquad (83)$$

The corresponding sampled-data loop gain is easily calculated.

$$T_s^*(s) = \frac{2\pi f_c / f_s}{e^{sT_s} - 1} \qquad (84)$$

In Eq. (84), the delay ε has already been made to vanish. The crossover frequency of the state-space averaged loop gain, the frequency at which $|T(s)|=1$, is f_c, and the switching frequency is f_s. These two functions are plotted in Fig. 18 in the form of Bode plots, from which stability information can be easily obtained. Contrary to the state-space averaged prediction, the sampled-data loop gain indicates that instability can indeed occur. In fact, the case shown is on the verge of instability. The phase of the sampled loop gain falls to -180° just as the magnitude reaches one, at one-half the switching frequency. A condition for the maximum value of f_c for stability can be easily derived from Eq. (84).

$$f_c < \frac{f_s}{\pi} \quad \text{for stability} \qquad (85)$$

Of course, for an adequate stability margin, the value of f_c chosen must be considerably below the maximum allowable.
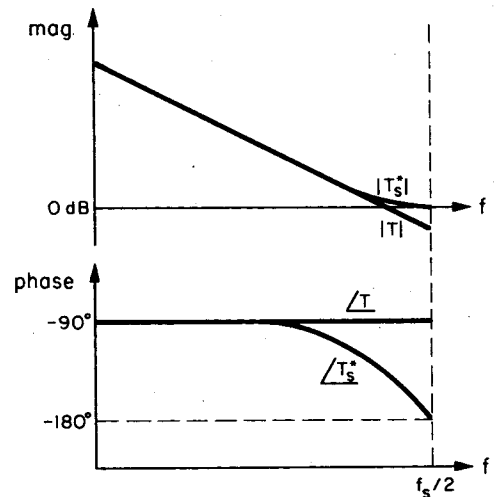

Figure 18. *State-space averaged and sampled-data loop gains for a single-pole system.*

The relationship between the sampled-data and state-space averaged loop gains given in Eq. (82) is of mainly qualitative interest, providing a visualization of the connection between the two. Another, more quantitative relationship can also be developed, based on the equivalent representation of the sampled-data loop gain $T_s^*(s)$ given in Eq. (77), repeated here as Eq. (86).

$$T_s^*(s) = H_e^T (e^{sT_s}I - e^{AT_s})^{-1} e^{AT_s} K T_s \qquad (86)$$

The straight-line approximation permits the replacement of the exponential matrix e^{AT_s} by the first two terms of its Taylor series expansion. Suppose the exponential form e^{sT_s} is similarly approximated by the first two terms of its Taylor series. This step is equivalent to

364

the assumption that the frequencies of interest are much less than the switching frequency.

$$e^{sT_s} \approx 1 + sT_s \ , \ sT_s \ll 1 \qquad (87)$$

With these approximations the sampled-data loop gain $T_s^*(s)$ can be rewritten in an approximate form.

$$T_s^*(s)\Big|_{e^{sT_s} \to 1+sT_s} \approx H_e^T(sI-A)^{-1}(I+AT_s)K \qquad (88)$$

The matrix $I+AT_s$ acts as a correction to the vector K. Owing to the straight line approximation, this correction is often small, and may be assumed negligible with only a small loss of accuracy.

$$T_s^*(s)\Big|_{e^{sT_s} \to 1+sT_s} \approx H_e^T(sI-A)^{-1}K = T(s) \qquad (89)$$

Thus, with this transformation, $e^{sT_s} \to 1+sT_s$, the sampled-data loop gain is transformed, to a good approximation, into the state-space averaged loop gain. As a test of this relation, consider the previous example, which treated the specific case of a state-space averaged loop gain with a single pole. An application of the transformation to the sampled-data loop gain of Eq. (84) should result in the recovery of the state-space averaged loop gain.

$$T_s^*(s) = \frac{2\pi f_c/f_s}{e^{sT_s} - 1} \to \frac{2\pi f_c/f_s}{sT_s} = \frac{2\pi f_c}{s} \qquad (90)$$

The last expression matches the state-space averaged form Eq. (83), and the transformation is verified for this case.

Thus, the sampled-data and state-space averaged loop gains are approximately related by the transformation $e^{sT_s} \to 1+sT_s$. Recall that the sampled-data and discrete modeling loop gains were similarly related by a transformation $e^{sT_s} \to z$. There is a difference between these two cases, however. The relationship between discrete modeling and sampled-data modeling is valid for all frequencies, reflecting the fact that the accuracies of the two techniques are comparable. However, the result of a transformation of a sampled-data loop gain via the substitution $e^{sT_s} \to 1+sT_s$ agrees with the original only at frequencies which are low compared to the switching frequency. Otherwise, the transformation is no more than a change of variables, with "s" at the end no longer being the true complex frequency. This restriction reflects the fact that the two methods only agree at low frequencies, with state-space averaging losing accuracy at higher frequencies.

The relationships between the sampled-data and state-space averaged models having been developed, it is well to conclude this subsection with a review of the origin of the difference between the two, specifically, the sampled-data model's increased high-frequency accuracy. Both techniques utilize the straight-line approximation, which allows the time-varying portions of the converter state matrix and forcing vector to be neglected, with only their average values being kept. However, the sampled-data technique stops at this point, retaining the pulsed nature of the duty ratio modulation function, while state-space averaging continues by replacing this pulse string with a smooth function. Thus, state-space averaging assumes that feedback can be

applied continuously, at any frequency, while the sampled-data technique correctly asserts that control can be exercised at only one moment in each switching cycle. This property increases a regulator's tendency to oscillate at high frequencies, since the controller may not be able to act quickly enough in response to state variations to restrain them. The recognition of this tendency in the sampled-data model, and its neglect in state-space averaging, are the origins of the differences between the two methods.

7.3 Properties of the sampled-data loop gain

The previous two subsections have emphasized the relationships between the new sampled-data modeling technique and the discrete and state-space averaged methods. In this present section, attention will be focussed solely on the sampled-data method, and in particular on the sampled-data loop gain. In many of its applications, for example, when displayed on Bode or Nyquist plots, the loop gain is considered to be a function not of the complex variable s, as it has been so far in this thesis, but rather of the frequency f. The discussion here will also restrict the loop gain's dependence to this range.

$$s = j2\pi f \qquad (91)$$

When considered as a function of frequency, the sampled-data loop gain possesses certain general properties which cause its plotted characteristic to be quite striking. These features are readily discernable from a particular representation of this function. This form, derived in Section 7.1, is repeated here as Eq. (92).

$$T_s^*(j2\pi f) = H_e^T(e^{j2\pi f/f_s}I - e^{AT_s})^{-1}e^{AT_s}KT_s \qquad (92)$$

One property of the sampled-data loop gain is derived by the replacement of the frequency f in Eq. (92) by $f+f_s$. Since $e^{j2\pi}=1$, the sampled-data loop gain is unchanged by this substitution, and is therefore periodic, with the switching frequency f_s as the period. Recognition of a second characteristic results from evaluation of Eq. (92) for the cases $f=0$ and $f=f_s/2$. Since $e^{j\pi}=-1$, and the other components are real vectors and matrices, in these two instances the loop gain T_s^* becomes purely real. The combination of this characteristic with the periodicity of the function implies that the sampled-data loop gain is real at each multiple of one-half the switching frequency.

Finally, consider the substitution $f \to f_s-f$ in Eq. (92).

$$T_s^*[j2\pi(f_s-f)] = H_e^T(e^{-j2\pi f/f_s}I - e^{AT_s})^{-1}e^{AT_s}KT_s \qquad (93)$$

This expression also results from the evaluation of the complex conjugate of the loop gain at the frequency f.

$$\overline{T_s^*[j2\pi f]} = H_e^T(e^{-j2\pi f/f_s}I - e^{AT_s})^{-1}e^{AT_s}KT_s \qquad (94)$$

This step used the fact that the conjugate of a matrix inverse is the inverse of its conjugate. The resulting equality reveals two symmetries of the sampled-data loop gain.

$$T_s^*[j2\pi(f_s-f)] = \overline{T_s^*[j2\pi f]} \qquad (95)$$

Consideration of the magnitudes of the two expressions in Eq. (95) shows that the magnitude of the sampled-data loop gain possesses even symmetry about one-half the switching frequency. The imaginary component of this equation, on the other hand, implies that the imaginary part of the sampled-data loop gain must be odd about one-half the switching frequency. Hence, the phase is odd about its value at one-half the switching frequency. This particular value of the phase must be a multiple of 180°, since, as was shown earlier, the loop gain is real at this frequency.

The combination of these three findings with the low-pass nature of switching converters results in a picture of the sampled-data loop gain something like that in Fig. 19. This general figure is quite useful for the determination of certain design implications of the sampled-data loop gain. For example, it is evident from this figure that the highest possible loop gain crossover frequency is one-half the switching frequency: if the crossover frequency were any higher, the loop gain would never fall below unity magnitude, and instability would be unavoidable. This property is due to the fact that control is only exercised once in each switching cycle; the most rapidly varying signal which can be propagated through this discrete controller has a period of twice the switching period.
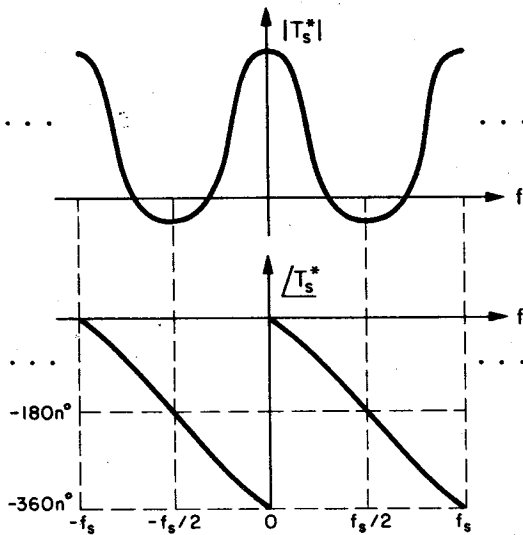

Figure 19. *General features of the sampled-data loop gain.*

This section has compared the new sampled-data modeling technique with the discrete modeling and state-space averaging methods, and has determined some general properties of the sampled-data loop gain. As a result of these exercises, the relationships among these three techniques have become clearer, and the position of sampled-data modeling among them has been made more evident.

6. CONCLUSIONS

In this paper, the development and high-frequency predictions of two switching regulator analysis methods, state-space averaging and discrete modeling, were compared. As a result of this comparison, a new modeling technique, the sampled-data method, was developed.

In Section 2, an equation describing the small-signal behavior of switching converters was developed. An important feature of this equation is that, other than a small-signal assumption used to obtain a linear equation, no approximations are required in its derivation. While too complicated to be directly useful in switching converter modeling, this equation can serve as a basis from which various modeling techniques can be developed.

State-space averaging, a widely used modeling scheme, was treated in Section 3. Its governing idea is the modeling of a switching regulator by a linear, time-invariant, matrix differential equation. Examination of its derivation revealed that, besides the small-signal assumption required for linearity, two modifications are involved. The first is related to the straight-line approximation, which is known to be an excellent approximation for switching converters. The second modification involves the smoothing of a pulsed driving signal into a continuous function. No justification is readily apparent for this step, and this approximation was noted as a potential limitation on the high-frequency capability of the state-space averaged technique.

In Section 4, the discrete modeling technique was discussed. Rather than using a continuous model, it represents a regulator by a linear, shift-invariant matrix difference equation. It was seen that only the small-signal approximation is used in its derivation. Thus, this modeling technique is expected to maintain excellent accuracy even at high frequencies. However, the method's unusual form makes its application difficult for someone unaccustomed to discrete systems, and does not convey the continuous nature of switching converter waveforms.

A feedback arrangement known as current-programming was introduced in Section 5. This regulation method is known to possess a well-defined high-frequency instability, and is thus a natural choice for a test of the high-frequency capabilities of state-space averaging and discrete modeling. When applied to this system, state-space averaging fails to predict the instability, thus confirming the doubts concerning its high-frequency capability. On the other hand, discrete modeling correctly predicts the current-programming instability, and can also be used successfully to investigate other aspects of current-programming. A generalization of this discussion led to the conclusion that the differences in predictions between these two methods are not limited to current-programmed regulators, but appear in a variety of systems. Thus, the stature of discrete modeling is enhanced, but its basic problem, an unfamiliar, inconvenient model representation, remains.

There was thus ample motivation to find a model with the form of state-space averaging and the accuracy of discrete modeling. Re-examination of the development of state-space averaging suggested that while the

straight-line approximation is a good one, the smoothing of the pulsed driving function is evidently unjustified. By use of only the straight-line approximation, a new model was developed in Section 6. The new method is called the sampled-data technique, because its form is that of a sampled-data system. The increased accuracy of the new model compared with state-space averaging was demonstrated by its ability to predict correctly the current-programming instability.

In Section 7, various relationships were developed between the new sampled-data model and the discrete and state-space averaged methods, and properties of the sampled-data loop gain were uncovered. The sampled-data and discrete models were seen to be two representations of the same system, via the transformation $z = e^{sT_s}$, as long as the straight-line approximation holds. On the other hand, comparison of the sampled-data and state-space averaged models showed that the sampled-data technique differs from state-space averaging only in the presence of a sampler in the feedback loop. This recognition led to the interpretation of state-space averaging as a low-frequency limiting case of the sampled-data method, approximately related to it by the transformation $e^{sT_s} \to 1+sT_s$. The increased high-frequency accuracy of the sampled-data technique was traced directly to the smoothing of the pulsed driving function in the derivation of state-space averaging.

An examination of the sampled-data loop gain was then undertaken. It was seen that this loop gain, when considered to be a function of real frequency, is periodic, with the switching frequency as period, and that its imaginary part vanishes at each multiple of one-half the switching frequency. In addition, the magnitude of this loop gain displays even symmetry about one-half the switching frequency, while its phase is odd about its value at that frequency. From these properties, and the low-pass nature of switching converters, the general form of the sampled-data loop gain was determined, and was shown to be useful in the design process.

The findings discussed above are all consistent with the conclusion that the sampled-data analysis technique combines the accuracy of the discrete method with the continuous form of state-space averaging. Thus, this new technique is ideal for the investigation of many topics of interest involving switching regulators. Its continuous form mirrors the continuous nature of actual switching regulator waveforms, and its predictions can be relied upon even for frequencies approaching one-half the switching frequency.

APPENDICES

The three appendices attached to this paper present background and, in some cases, derivations of important results which are used in this work. The subjects addressed in these sections are the properties of the z-transform, the application of the Laplace transform to sampled-data systems, and the relation between the z-transform and the Laplace transform descriptions of a sampling system.

Appendix A provides a brief presentation of the definition and important properties of the one-sided z-transform used in this paper. Also, interpretations of several simple z-transforms are given, in order to provide some "feel" for this important tool.

The properties of the Laplace transforms of sampled functions are reviewed in Appendix B. This appendix treats two subjects. First, the Laplace transform of a sampled function is defined and evaluated in three different but equivalent ways. Second, it is demonstrated that the sampling operation does not affect the transform of a previously sampled signal.

Finally, in Appendix C, a connection is made between the first two appendices. Specifically, for a sampled function, a transformation is derived which relates the z-transform of the waveform to the Laplace transform of the same function.

A. Definition and properties of one-sided z-transforms

For a sequence of numbers $x(n)$, $n = ..., -1, 0, +1, ...$, define the one-sided z-transform $Z[x(n)]$.

$$Z[x(n)] = X(z) = \sum_{n=0}^{\infty} x(n)z^{-n} \qquad (A.1a)$$

$$= x(0) + x(1)z^{-1} + x(2)z^{-2} + ... \qquad (A.1b)$$

Linearity is obvious.

$$Z[ax(n) + by(n)] = aX(z) + bY(z) \qquad (A.2a)$$

$$Z[x(n)] = X(z) \qquad Z[y(n)] = Y(z) \qquad (A.2b)$$

A shift rule for this z-transform is also easily established.

$$Z[x(n+1)] = x(1) + x(2)z^{-1} + x(2)z^{-2} + ... \qquad (A.3a)$$

$$= z\{Z[x(n)] - x(0)\} \qquad (A.3b)$$

An analysis of some simple examples of z-transforms can aid in the extraction of content from this important tool.

$$X(z) = \frac{1}{z - a} = \frac{z^{-1}}{1 - z^{-1}a} \qquad (A.4a)$$

$$= z^{-1}(1 + az^{-1} + a^2 z^{-2} + ...) \qquad (A.4b)$$

The sequence corresponding to this transform can be written down directly.

$$x(n) = \{0, 1, a, a^2, ...\} \qquad (A.5)$$

Examination of this sequence for various choices of the pole position a provides an interpretation of the transform.

Cases	
$|a| < 1$	decaying sequence, stable
$|a| > 1$	growing sequence, unstable
$a = -1$	subharmonic oscillation $\{1,-1,1,-1,...\}$
$a = 0$	finite sequence ("finite-settling time")

B. Laplace transforms of sampled signals

Consider a function $v(t)$ with associated Laplace transform $V(s)$. Passage of this waveform through a sampler with period T_s gives a string of delta functions.

$$v^*(t) = v(t)T_s\delta_{T_s}(t) \qquad \text{(B.1a)}$$

$$\delta_{T_s}(t) = \sum_{n=-\infty}^{\infty} \delta(t-nT_s) \qquad \text{(B.1b)}$$

The problem is to evaluate the Laplace transform $V^*(s) = L\{v^*(t)\}$ associated with $v^*(t)$. There are several ways to proceed [8], and three different approaches will be summarized in this appendix.

The first method works with the time domain representation of $v(t)$. The result is an infinite series which represents the sampled-data Laplace transform wherever the series converges.

$$V^*(s) = T_s \sum_{n=0}^{\infty} v(nT_s)e^{-snT_s} \qquad \text{(B.2)}$$

The other two methods use the Laplace transform of $v(t)$ in their representations. In these techniques, the complex multiplication theorem for Laplace transforms (the counterpart of the convolution theorem) is applied to the defining Eq. (B.1), yielding a line integral in the complex s-plane. This integral can be evaluated by use of residue techniques in two ways, depending on whether the contour path is closed to the right or to the left. When closed to the right, the sampled Laplace transform is given as an infinite summation of shifted versions of the unsampled transform.

$$V^*(s) = \sum_{n=-\infty}^{\infty} V(s+jn\omega_s) \qquad \text{(B.3)}$$

Of course, the sum must converge for this statement to have meaning. When the integration contour is closed to the left, the sampled Laplace transform is evaluated as a sum over the poles of the unsampled Laplace transform, plus a correction term resulting from the extension of the contour. Rather than the general result, only a case of special interest to this paper is presented. Specifically, suppose that $V(s)$ represents a high-order integrator, with an additional small delay ε.

$$V(s) = \frac{e^{-\varepsilon s}}{s^m}, \quad m=1, 2, 3,... \qquad \text{(B.4)}$$

Then the sampled Laplace transform is the difference of two contributions.

$$V^*(s) = T_s \sum_{\substack{\text{poles } s_n \\ \text{of } V(s)}} \left[\text{residue of } \frac{V(p)}{1-e^{-(s-p)T_s}} \bigg|_{p=s_n} \right] - I \qquad \text{(B.5a)}$$

$$I = \begin{cases} T_s & \text{if } m=1 \\ \dfrac{(-\varepsilon)^{m-1}}{(m-1)!}T_s & \text{if } m>1 \end{cases} \qquad \text{(B.5b)}$$

Note that for $m>1$, the additional term I vanishes for $\varepsilon \to 0$, but that it does not vanish for $m=1$. This behavior is the exact mathematical analog of the physical arguments presented earlier in this paper. Specifically, a delta function cannot propagate instantaneously

through an integrator of order greater than one, so the addition of a small delay in series with the integrator makes no great difference in the propagated signal. However, this addition makes a profound difference in the case of a simple integrator, $m=1$, because instantaneous transmission of a delta function does occur for this system. The sampled Laplace transform for this situation is used extensively in this paper, and is easily evaluated from the above equations.

$$V(s) = \frac{e^{-\varepsilon s}}{s} \qquad \text{(B.6a)}$$

$$\lim_{\varepsilon \to 0} V^*(s) = \frac{T_s}{e^{sT_s} - 1} \qquad \text{(B.6b)}$$

Finally, it is shown in the following demonstration that a sampled Laplace transform can be factored out of any additional sampling operation, provided the samplers are synchronous.

$$[A(s)B^*(s)]^* = \sum_{n=-\infty}^{\infty} A(s+jn\omega_s)B^*(s+jn\omega_s) \qquad \text{(B.7)}$$

This first step uses the second form of the sampled Laplace transform found earlier. The second, sampled transform in this expression is now expanded.

$$[A(s)B^*(s)]^* = \sum_{n=-\infty}^{\infty} \{A(s+jn\omega_s) \times \sum_{m=-\infty}^{\infty} B(s+jn\omega_s+jm\omega_s)\} \qquad \text{(B.8)}$$

This expression is readily factored by the substitution $l=m+n$.

$$[A(s)B^*(s)]^* = \sum_{n=-\infty}^{\infty} A(s+jn\omega_s) \sum_{l=-\infty}^{\infty} B(s+jl\omega_s) \qquad \text{(B.9a)}$$

$$= A^*(s)B^*(s) \qquad \text{(B.9b)}$$

This is the desired result. This factorization is used in the development of the sampled-data model in this paper.

C. Relationship between z-transform and sampled Laplace transform

Consider a time function $u(t)$ with Laplace transform $U(s)$. Suppose this function is passed through a sampler with period T_s, as defined in Appendix B.

$$u^*(t) = u(t)T_s\delta_{T_s}(t) = u(nT_s)T_s\delta_{T_s}(t) \qquad \text{(C.1a)}$$

$$\delta_{T_s}(t) = \sum_{n=-\infty}^{\infty} \delta(t-nT_s) \qquad \text{(C.1b)}$$

In Appendix B, three expressions for the Laplace transform $U^*(s)$ of this sampled signal were displayed. The first of those is particularly useful here.

$$U^*(s) = T_s \sum_{n=0}^{\infty} u(nT_s)e^{-sT_s n} \qquad \text{(C.2)}$$

Now the sampled values $T_s u(nT_s)$ form a sequence of numbers, so it is possible to define a z-transform for the sampled function $u^*(t)$.

$$Z[u^*(t)] = U_z(z) = \sum_{n=0}^{\infty} T_s u(nT_s)z^{-n} \qquad \text{(C.3)}$$

Comparison of Eqs. (C.2) and (C.3) reveals the relationship between the Laplace transform of a sampled function and the z-transform of the same function.

$$U^*(s) = U_z(z = e^{sT_s}) \qquad \text{(C.4)}$$

In particular, the poles s_p of $U^*(s)$ are related to the poles z_p of $U_z(z)$ by a simple relation.

$$z_p = e^{s_p T_s} \qquad \text{(C.5)}$$

This correspondence is used, in Section 7, to investigate the relationship between sampled-data modeling and discrete modeling.

REFERENCES

[1] Slobodan Ćuk, "Modelling, Analysis, and Design of Switching Regulators", PhD thesis, California Institute of Technology, November 1976; also, NASA Report CR-135174.

[2] Dennis J. Packard, "Discrete Modeling and Analysis of Switching Regulators", PhD thesis, California Institute of Technology, May 1976; also, Report No. M76-43, Hughes Aircraft Co., Aerospace Groups, Culver City, Calif.

[3] Shi-Ping Hsu, Art Brown, Loman Rensink, and R. D. Middlebrook, "Modelling and Analysis of Switching Dc-to-Dc Converters in Constant-Frequency Current-Programmed Mode", IEEE Power Electronics Specialists Conference, 1979 Record, pp. 284-301 (IEEE Publication 79CH1416-3 AES).

[4] R. D. Middlebrook, "Modelling and Design of the Ćuk Converter", Proc. Sixth National Solid-State Power Conversion Conference (Powercon 6), pp. G3.1-G3.14, May 1979.

[5] W. M. Polivka, P. R. K. Chetty, and R. D. Middlebrook, "State-Space Average Modelling of Converters with Parasitics and Storage-Time Modulation", IEEE Power Electronics Specialists Conference, 1980 Record, pp. 119-143 (IEEE Publication 80CH1529-7).

[6] Slobodan Ćuk and Robert W. Erickson, "A Conceptually New High-Frequency Switched-Mode Amplifier Technique Eliminates Current Ripple", Proc. Fifth National Solid-State Power Conversion Conference (Powercon 5), pp. G3.1-G3.22, May 1978.

[7] Loman Rensink, Art Brown, Shi-Ping Hsu, and Slobodan Ćuk, "Design of a Kilowatt Off-Line Switcher Using a Ćuk Converter", Proc. Sixth National Solid-State Power Conversion Conference (Powercon 6), pp. H3.1-H3.26, May 1979.

[8] Eliahu I. Jury, Sampled-Data Control Systems, John Wiley & Sons, 1958.

[9] Cecil W. Deisch, "Simple Switching Control Method Changes Power Converter into a Current Source", IEEE Power Electronics Specialists Conference, 1978 Record, pp. 300-306 (IEEE Publication 78CH1337-5 AES).

[10] A. Capel, G. Ferrante, D. O'Sullivan, and A. Weinberg, "Application of the Injected Current Model for the Dynamic Analysis of Switching Regulators with the New Concept of LC^3 Modulator", IEEE Power Electronics Specialists Conference, 1978 Record, pp. 135-147 (IEEE Publication 78CH1337-5 AES).